Application of GPS to geodesy: A combination problem in estimation and large-scale hypothesis testing

by

Yung Chih Patrick Hwang

A Thesis Submitted to the
Graduate Faculty in Partial Fulfillment of the
Requirements for the Degree of
MASTER OF SCIENCE

Major: Electrical Engineering

Iowa State University
Ames, Iowa

1983

TABLE OF CONTENTS

		Page
I.	INTRODUCTION	1
II.	BACKGROUND IN KALMAN FILTER THEORY	3
	A. The Discrete Kalman Filter	3
	B. The Magill Adaptive Filter	6
	C. Adaptive Estimation in Multiple Hypothesis Testing	9
III.	NAVSTAR GPS AND ITS APPLICATIONS IN GEODESY	12
	A. The Global Positioning System	12
	B. GPS and Centimeter-Level Geodesy	16
IV.	THE INCREMENTAL GPS GEODESY MODEL WITH COMPUTER-SIMULATED RESULTS	18
	A. Single Satellite in a Plane	18
	B. Accounting for Clock Error	25
	C. Three-Dimensional Geometry	29
	D. Effects of Increased Sampling Rates	36
V.	COMPUTATIONAL CONSIDERATIONS FOR LARGE INTEGER AMBIGUITY IMPLEMENTATIONS	40
	A. Maximum Likelihood	41
	B. The Augmented Kalman Filter	48
	C. A Comparison of the Maximum Likelihood and the Augmented Kalman Filter Approaches	52
VI.	CONCLUSIONS	56
	A. Summary of Results	56
	B. Topic Suggestions for Future Research	57
VII.	REFERENCES	59
VIII.	ACKNOWLEDGMENTS	61

Page

IX. APPENDIX A: INITIALIZING THE AUGMENTED KALMAN FILTER 62

X. APPENDIX B: COMPUTER SIMULATION PROGRAMS 65

A. One-dimensional Single-Satellite Model with Planar Geometry 67

B. Three-dimensional Four-Satellite Model (Preliminary Estimation with Maximum Likelihood Method) 69

C. Three-dimensional Four-Satellite Model (Preliminary Estimation with Augmented Kalman Filter) 76

I. INTRODUCTION

The problem of relative positioning in geodesy can generally be regarded as "the determination of the location of one point with respect to another, either by measuring directly between the two points or by measuring indirectly from two points to extraterrestrial objects" [1]. The more frequently encountered problem in geodetic surveying, however, of finding the direction and distance between two given points is just the inverse case of the above.

The idea of using satellites for geodetic surveying is by no means a new one [2]. The advantages of this extraterrestrial method clearly surpass those of terrestrial alternatives in operating environments affording only reduced visibilities due to terrain, weather, or sheer distances. Recent developments in satellite geodesy have been focused on a promising new navigational scheme known as the Global Positioning System (GPS). This scheme, which incorporates state-of-the-art technology from various disciplines, is planned to be operational by the later part of the decade. Although the normal differential mode of the GPS operation contends with mere accuracies of several meters, recently-developed radio interferometric techniques have reported the achievement of centimeter-level precision based on data gathered over an hour or two of observation time [3,4].

This project constitutes an investigation based on an alternative approach to the GPS geodesy problem with the primary objective of reducing the required observation time through optimal processing and management of the data gathered. The ultimate goal naturally is to develop a

practical model for implementation through computer simulations leading up to eventual field testing. Using the differential position established by normal means as a coarse approximation, "fine-tuning" on the estimate can then be carried out on an incremental basis by timing on the carrier phase of the GPS signal instead of the usual coded modulation. This inevitably leads to the problem of ambiguity in the accumulated integer wavelengths, an inherent dilemma in measuring phase delay. Kalman filtering techniques are invoked to solve what will eventually be seen as a combination problem in estimation and multiple-hypothesis testing.

The two chapters following this one will cover relevant background material. Formulations and solutions to the Kalman filter and Magill adaptive filter are reviewed in Chapter II. The Global Positioning System and its involvement in satellite geodesy will be briefly discussed in the next chapter. Chapter IV covers the formulation of the incremental model with the solution to the integer wavelength ambiguity dilemma (to be referred simply as integer ambiguity). A one-dimensional example presented with computer simulated results serves as a tutorial that will be referred back to time and again for its clarity for analysis. Extension to a 3-dimensional GPS-like geometric model will also be pursued here. Chapter V addresses the massive computational burden generated by the Magill adaptive filter solution. Two approaches are formulated, one of which is a generalized version of the original Magill solution. They are compared and shown to yield the same results under certain special conditions.

II. BACKGROUND IN KALMAN FILTER THEORY

In this application of the Global Positioning System to geodesy, we encounter a typical problem of "recovering" signals that are immersed in noise. One of the most powerful statistical tools available today in filtering out noise is an algorithmic scheme known as the Kalman filter. The essentials to the theory of this well-proven method will make up the first topic of this chapter, followed by an extension of the filter to an adaptive scheme in the next section. The adaptation of the latter to our application problem at hand will, in turn, be the topic of the last section.

A. The Discrete Kalman Filter

The discrete Kalman filter is essentially a recursive algorithm that estimates a random process from a set of noisy measurement data that is linearly related to the process itself. The filter is optimal for Gaussian processes; otherwise, it is only optimal as a linear filter in a least squares sense.

This technique is credited to R. E. Kalman who, in 1960, provided an alternative solution to the more computationally restrictive Wiener filter of an earlier generation. Since the theory of the Kalman filter is adequately documented in the literature, in particular, Kalman's original paper [5] as well as several other reference texts [6-8], it is simply sufficient here to provide a brief summary of the formulation and solution to the discrete version of the filter.

The random process and measurement models are given by the following

relationships:

$$x_{k+1} = \Phi_k x_k + w_k \tag{2.1}$$

$$z_k = H_k x_k + v_k \tag{2.2}$$

An explanation of the notation here is in order. The subscript k denotes the value of a variable at time t_k. Additionally:

x_k = the process state vector

z_k = the measurement vector

Φ_k = the state transition matrix

H_k = the linear connection matrix between the measurement and the state

w_k = process noise (Gaussian white sequence) with covariance Q_k

v_k = measurement noise (Gaussian white sequence uncorrelated with the w_k sequence) with covariance R_k

The Kalman filter equations are given here in the order of the computational sequence and are summarized in a block diagram given in Figure 2.1.

$$K_k = P_k^- H_k^T [H_k P_k^- H_k^T + R_k]^{-1} \tag{2.3}$$

$$\hat{x}_k^+ = \hat{x}_k^- + K_k(z_k - H_k \hat{x}_k^-) \tag{2.4}$$

$$P_k^+ = [I - K_k H_k] P_k^- \tag{2.5}$$

$$\hat{x}_{k+1}^- = \Phi_k \hat{x}_k^+ \tag{2.6a}$$

$$P_{k+1}^- = \Phi_k P_k^+ \Phi_k^T + Q_k \tag{2.6b}$$

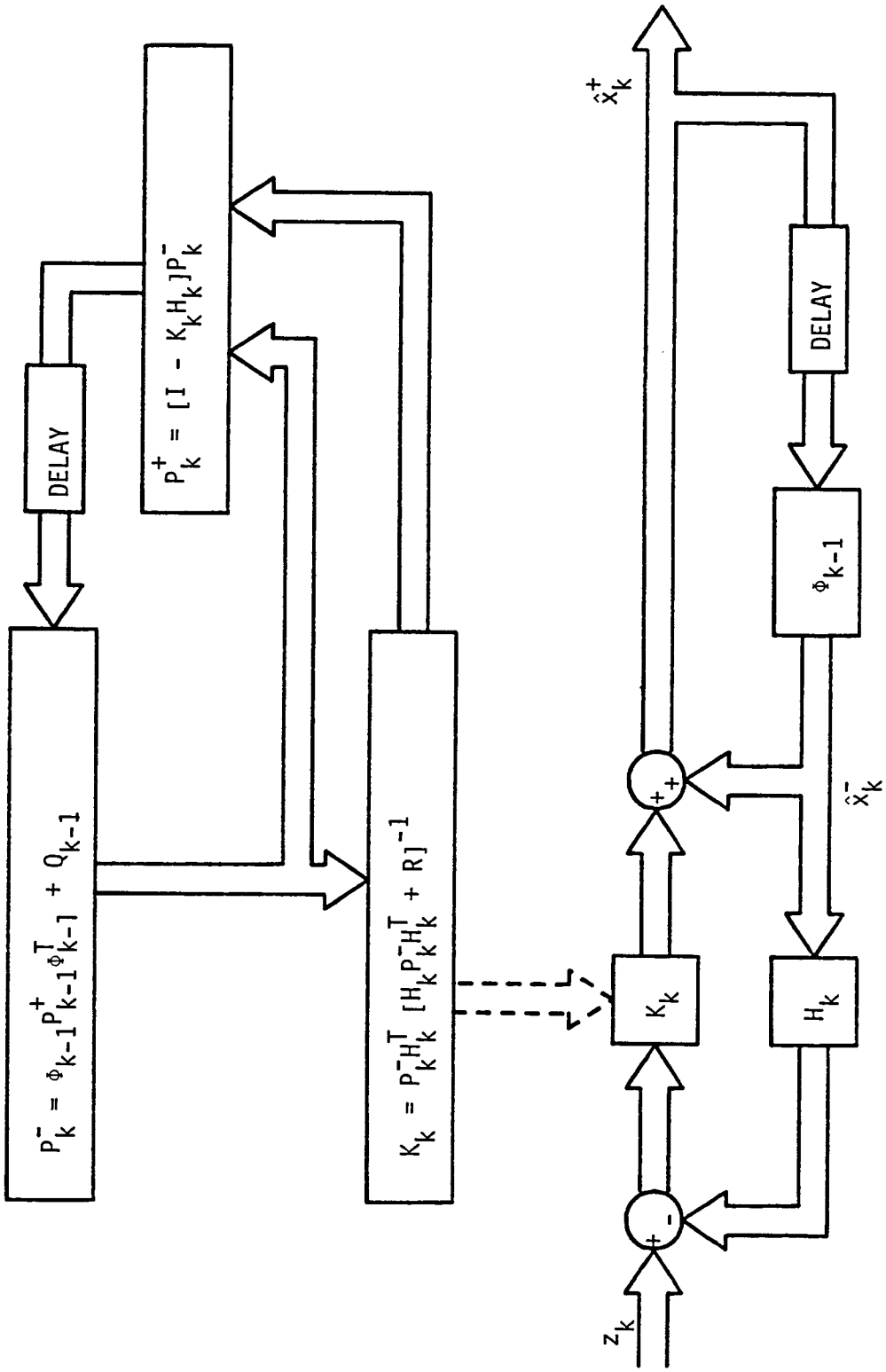

Figure 2.1. The discrete Kalman filter algorithm

The circumflex denotes that the corresponding variable is an estimate. The initial values of the filter are:

$\hat{x}_0^-$ = mean value of x_0

P_0^- = error covariance associated with $\hat{x}_0^-$

In eqs. 2.3-2.6, K_k denotes the Kalman gain which is used to weight the measurement residual $(z_k - H_k\hat{x}_k^-)$ and P_k is the error covariance matrix associated with the state vector. The superscripts used on x and P represent a priori and updated versions of the respective quantities.

In the two decades since the Kalman filter was first introduced, a lot of activity has taken place involving applications, refinements, and adaptations of the filter. Applications have diversified substantially from the original settings of aerospace and navigation to many other areas which include industrial, geophysical and power systems, and even demography [9]. Extended and linearized versions of the filter have arisen to accommodate nonlinear dynamics. And perhaps the most relevant development of all, with regard to this research project, is an adaptive scheme based on a paper published in 1965. The adaptation of this scheme to our application follows in the next section.

B. The Magill Adaptive Filter

There are cases, on occasion, where complete knowledge of a certain parameter related to the filter becomes elusive to the analyst for any one of a variety of reasons. In such instances, an adaptive estimator, with the ability to adapt itself to the initially unknown portion of the model, can be a particularly useful approach in solving for the unknown parameter.

The adaptive estimator based on a scheme proposed by D. T. Magill [10] calls for an implementation of a parallel bank of Kalman filters, each modeled around a particular realization of the unknown parameter. It is obvious, then, that the unknown parameter must necessarily have a finite number of realizations which are discrete in nature as well. The output from each and every filter element in the bank is then properly weighted and summed to give a blended output. The degree of "correctness" is reflected in the weighting factor which is itself rather appropriately defined as the conditional probability that the parameter realization is correct given the information from the measurement sequence. A summary of this scheme is provided in Figure 2.2, where z_k^* denotes the measurement sequence $z_0, z_1, \ldots, z_k$.

No attempt will be made here to review the mathematical derivations leading to Magill's solution. However, the following are the key results of his paper (see reference [6] sec. 9.2):

$$p(\alpha_i | z_k^*) = \frac{p(z_k^* | \alpha_i)\ p(\alpha_i)}{\sum_{j=1}^{N} p(z_k^* | \alpha_j)\ p(\alpha_j)} \tag{2.7}$$

$$p(z_k^* | \alpha_i) = \frac{1}{[2\pi(H_k P_k^- H_k^T + R_k)]^{1/2}} \exp\left[-\frac{(z_k - H_k \hat{x}_k^-)^2}{2(H_k P_k^- H_k^T + R_k)}\right] p(z_{k-1}^* | \alpha_i) \tag{2.8}$$

The recursive form of eq. 2.8 is perhaps the attractive feature that contributes most to the practicality of this implementation. The notation used here is consistent with that introduced in the previous section. It should also be noted that $(z_k - H_k \hat{x}_k^-)$ and $(H_k P_k^- H_k^T + R_k)$ found in the above equations are quantities that are computed in the regular

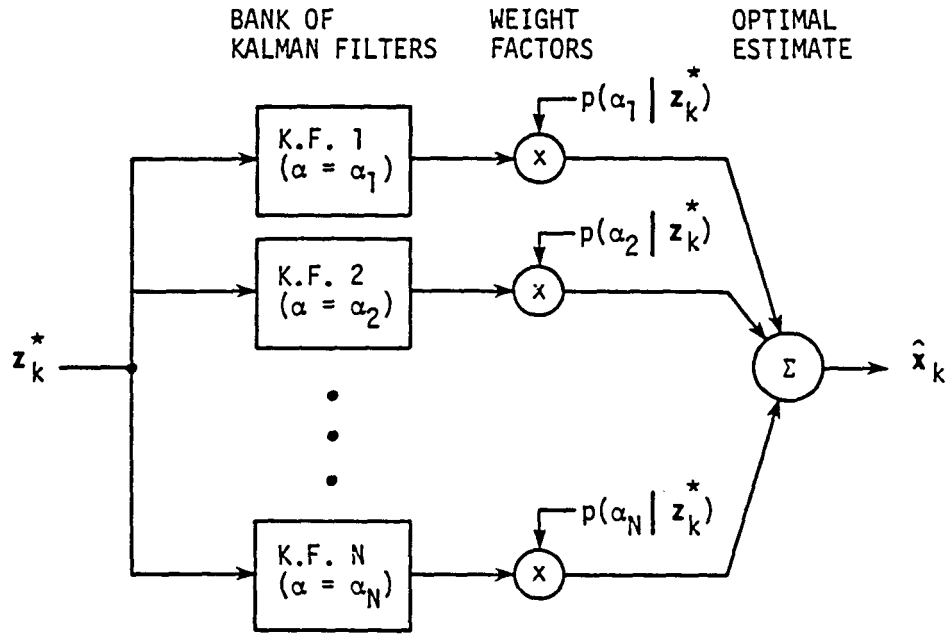

Figure 2.2. The Magill adaptive filter

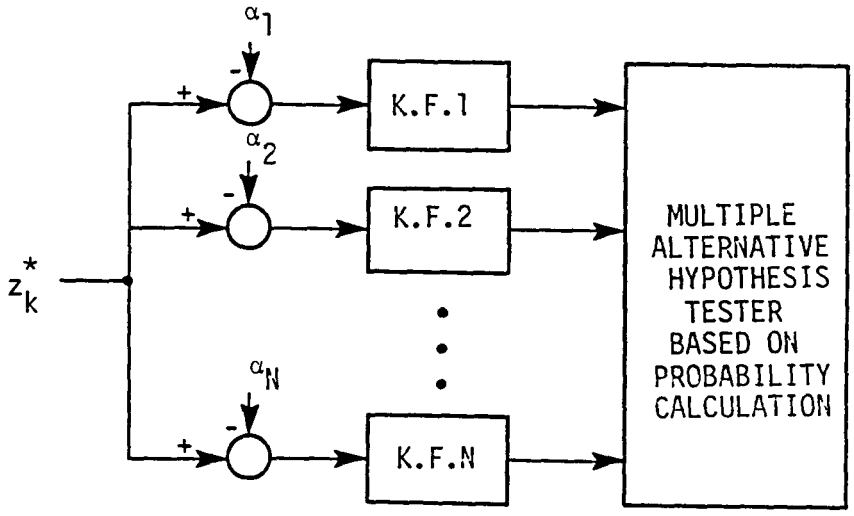

Figure 2.3. Multiple hypothesis tester derived from the Magill adaptive scheme

filter equations given in eqs. 2.3 and 2.4. At the risk of a slight deficiency in notation, $p(\cdot)$ in eqs. 2.7 and 2.8 has been used to represent both probability and probability density. The normal use of upper case P for the former is hereby waived to avoid confusion with its use in representing the state error covariance matrix in the Kalman filter algorithm. In any case, it should be clear from the context as to which interpretation applies in these equations.

C. Adaptive Estimation in Multiple Hypothesis Testing

The Magill adaptive filter, also known as the partitioned adaptive filter, is widely used in parameter identification problems where the "parameter" involved is usually one of the covariance quantities. Brown [11], however, has proposed that this parallel processing technique can be applied to problems where the unknown parameter is an additive bias in the measurement model. This scheme, as is given in Figure 2.3, clearly represents the recursive version of a multiple hypothesis tester. Each element in the parallel bank operates on the same measurement sequence but adjusts it by the appropriate "hypothesized" amount of bias before processing. Since the hypothesis appears only in the measurement model, the gain and covariance structures of the filters are uniform throughout the parallel bank. This commonality is crucial in drastically reducing the amount of computational effort normally associated with the Magill adaptive scheme, especially if the set of hypotheses is large.

This adaptation brings about a happy congruence between the areas of estimation and detection theory. Nevertheless, a subtle difference in

emphasis remains between the two. In hypothesis testing, statistical decision theory calls for a decision to be made on the correct hypothesis and only the output of that element (in the parallel bank) need be considered. This differs from the significance of the blended output as seen from the point of view of adaptive estimation.

In the decision-making process, we need only consider the weighting factors $p(\alpha_i|z_k^*)$ as specified by eq. 2.7. Further simplifications may be obtained from considering the unconditional probability distribution of $p(\alpha_i)$ as uniform throughout the range of implementation, thereby allowing the use of $p(z_k^*|\alpha_i)$ (commonly known in statistical decision theory as the likelihood function) as the decision criterion. Also, eq. 2.8 can be expanded as a product to include the initial term, $p(z_{-1}^*|\alpha_i)$:

$$
\begin{aligned}
p(z_k^*|\alpha_i) = {} & A_k \exp\left[-\frac{(z_k - H_k\hat{x}_k^-)^2}{2(H_k P_k^- H_k^T + R_k)}\right] \cdot \\
& A_{k-1} \exp\left[-\frac{(z_{k-1} - H_{k-1}\hat{x}_{k-1}^-)^2}{2(H_{k-1} P_{k-1}^- H_{k-1}^T + R_{k-1})}\right] \cdot \\
& \cdots\cdots\cdots \\
& A_0 \exp\left[-\frac{(z_0 - H_0\hat{x}_0^-)^2}{2(H_0 P_0^- H_0^T + R_0)}\right] \qquad (2.9) \\
= {} & \prod_{j=1}^{k} A_j \exp\left\{\sum_{m=1}^{k} -\frac{(z_m - H_m x_m^-)^2}{2(H_m P_m^- H_m^T + R_m)}\right\}
\end{aligned}
$$

where:

$$A_j = 1/[2\pi(H_j P_j^- H_j^T + R_j)]^{1/2}$$

and $$p(z_{-1}^*|\alpha_i) = 1$$

In this particular implementation, A_j is independent of the hypothesis α_i. It is evident, then, that we can derive from eq. 2.9 a log-likelihood type function defined as

$$\sum_{m=1}^{k} - \frac{(z_m - H_m \hat{x}_m^-)^2}{2(H_m P_m^- H_m^T + R_m)} \tag{2.10}$$

In place of the likelihood function $p(z_k^* | \alpha_i)$, the parameter given by eq. 2.10 can be used to evaluate the decision in choosing among the hypotheses. It should be noted that in addition to a reduction in computational steps, the use of the above-formed likelihood function will also help relieve potential numerical problems (caused primarily by the exponentiation operation) sometimes encountered by the regular Magill adaptive scheme [12].

III. NAVSTAR GPS AND ITS APPLICATIONS IN GEODESY

The Global Positioning System is now spawning a host of new application ideas in geodesy-oriented problems as well as navigational ones. This chapter serves to provide what can only be a very brief overview of the many aspects involved in terms of characteristics and operations of the system. As a result, only those topics which are of any relevance to this project will be highlighted. In the second section of the chapter, potential applications of the GPS in geodetic surveying already under development will be reviewed.

A. The Global Positioning System

Fully designated as the Navigation Satellite Timing and Ranging Global Positioning System (NAVSTAR GPS), this project originated in the early 1970s, evolving out of a merger between two independent military research projects of the same nature. Its primary goal of providing global satellite passive ranging for navigational purposes, scheduled to be fully operational by the late 1980s, has certainly aroused anticipation in potential exploitation by the civilian community as well. Over the past decade since its inception, the originally-proposed 24-satellite scheme has been withered down to a considerably smaller one comprising a constellation of 18 satellites orbiting in half-synchronous trajectories inclined at 55 degrees to polar.

The basic mechanism employed by the GPS in its differential position determination scheme involves ranging from a known satellite position to the local receiver location by accurately timing the signal propagation

delay. The satellite position ephemerides are embedded in a 1500-bit navigation message periodically transmitted from the satellites. This information, available after processing by the user equipment, is only a very good approximation at best based on observational sightings of the satellite in question made by "upload" earth stations. By working the position determination problem in reverse since the "upload" locations are fixed and known, the ephemeris information carried in a satellite's data banks pertaining to itself is updated on a regular basis. The navigation message itself is coded by spread spectrum techniques and modulated on two carrier frequencies: approximately 1.2 and 1.5 GHz. The coding of the message with pseudorandom sequences reduces the effects of both intentional and unintentional signal interference.

The extremely high degree of precision demanded in timing the signal transit time is facilitated by the availablity of highly stable clocks with drifts in the order of one part in 10^{13} per day for a cesium standard. Receiver sets designed with restricted budgets in mind though may have to settle for more limited performance instead of such alternatives as rubidium or quartz. Even so, these clocks should provide more than adequate stability for the relatively short spans of timing operations involved. The inevitable problem of synchronization between the receiver clock and the coordinated satellite time standard, however, cannot be alleviated by accurate timing. It must instead be resolved by treating this clock bias error as an additional variable, often termed pseudorange, to compute in the position determination problem. Hence, to determine a position in 3-space, four satellite fixes are required to

perform the task.

The accuracy of the solution can be greatly enhanced by sighting well-placed satellites in the visible sky. It is intuitively evident, for example, drawing from an analogy on the problem of binocular ranging, that in having four satellites spatially clustered together as depicted in Figure 3.1a, the observation data obtained will be inferior, in terms of providing accuracy to the solution, to those gathered from four satellites that are distributed sparsely over the visible sky such as those shown in Figure 3.1b. The measure used to assess this "well-placed" quality in the geometry is known as the Geometric Dilution of Precision or GDOP. If more than four satellites are available at any one time, then choosing the satellites on the basis of minimizing the GDOP factor will lead to the most accurate results obtainable using the given satellites.

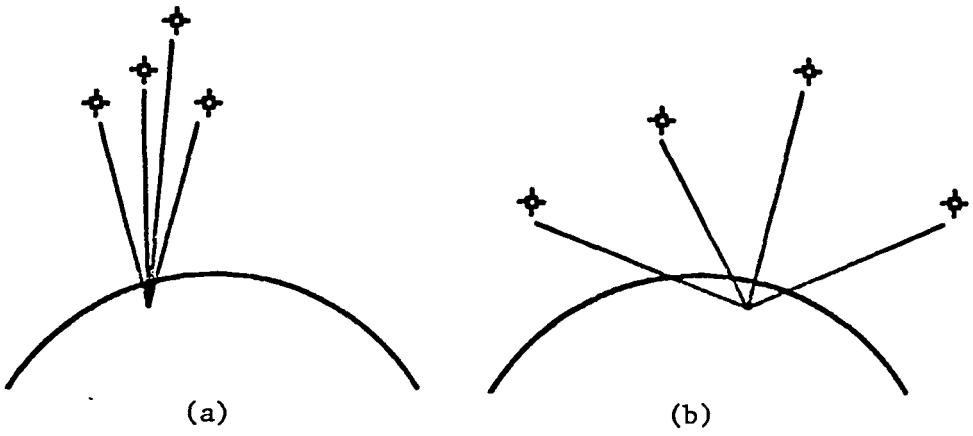

Figure 3.1. Satellite distributions that yield (a) high Geometric Dilution of Precision (GDOP), and (b) low GDOP (high accuracy)

Other sources of error encountered that affect the GPS system accuracy in ranging include:

(1) Undetermined ionospheric and tropospheric delays that have both the effects of reducing the speed of the propagating signal as well as causing refraction of the signal ray. The latter is especially critical when a satellite is at a low elevation. Atmospheric models have been formulated to compensate for these distortional effects.

(2) Group delay comprises of the uncertainties in the processing and passage of signals through the satellite equipment. These uncertainties can be predetermined experimentally from benchmark tests.

(3) Multipath resulting from the interference of signals following more than one propagation route.

(4) Receiver noise which also includes resolution errors primarily associated with the equipment itself.

Results from the field testing accomplished thus far have been very encouraging. Accuracies of a few meters have been reported as being achievable using the differential GPS mode [13,14]. Although the use of the GPS is certainly not restricted to position determination alone, this is the only relevant aspect of interest in our application to geodesy. There are many references pertaining to the characterization, development, and various other potential applications of the GPS available to the reader interested in delving further into the general subject [15,16].

B. GPS and Centimeter-Level Geodesy

The interest in using GPS for precision geodesy has recently begun to gain momentum as reflected in the growing number of papers covering the subject [3,4,17-19]. The research activity to date has been more or less dominated by interferometric methods which find their roots in radio astronomy. These methods are likely offshoots from the more established Very Long Baseline Interferometry (VLBI) technique using quasar sources developed for geodetic surveying nearly fifteen years ago.

The GPS's potential in achieving very high-resolution performance is derived from the stability of the signals transmitted from the satellites. In comparisons made with other advanced surveying techniques [17], all nonterrestrial in nature, GPS methods are expected to approach closest, in terms of precision and range, to the capabilities of terrestrial surveying techniques. This projection is based on current developments in GPS geodesy schemes which have shown centimeter-level precision capabilities. Several such receiver systems are now under development and should be commercially available in the near future. The pricing on these introductory units will naturally be very exclusive, although much more reasonable costs are expected when the GPS becomes fully operational towards the end of the decade.

Of the receiver systems capable of centimeter-level geodesy, the MACROMETER, a commercial outgrowth of the research work of Counselman and his colleagues (see references [18, 19]), has demonstrated to be the most promising on the basis of field test results carried out on prototype units. The operating procedure calls for recording the measurement

data on storage media at both ends of the baseline for typically an hour or two, and then batch-processing the accumulated data off-line at a central coordinating site. The processing may be roughly described as an iterative adjustment of the baseline vector until a "best fit" from the measurement data available is obtained.

Accuracies of 5 millimeters over short baselines under one kilometer and 1:170,000 resolution over longer baselines (around 100km) have been reported with this interferometric scheme [3]. No mention, however, of the relative observation time spans required in obtaining these results was given.

As an additional note, due to the significance of wavefront interference as the principal mechanism involved in this technique, the problems of multipath interference become irrepressibly crucial. Much research effort in this area, as such, has been concentrated on the study of antenna systems and their design.

Two other receiver systems, the SERIES and the GEOSTAR, currently less advanced in the developmental stage than the MACROMETER, are also pursuing the centimeter-level objective. Neither of these has yet to report any accomplishments in field testing.

IV. THE INCREMENTAL GPS GEODESY MODEL WITH COMPUTER-SIMULATED RESULTS

In order to achieve the very high degree of resolution sought after, the incremental GPS geodesy model approaches the position determination problem by way of using a coarse estimate attained via some other means to narrow down the uncertainty, and then improving on it in an incremental fashion. The formulation of this model which forms the framework of the project will be the topic of detailed discussion in this chapter. The ordering of the sections in accordance with increasing complexity is, not surprisingly, also the chronological order of development in the research work done. The simplest case of a single satellite in a one-dimensional position determination problem will be formulated in the first section. The modeling of the clock error and its resulting effects are to be discussed in the next section. In a third section, the full-blown three-dimensional problem with a realistic geometry will be formulated and its results discussed. The last section of this chapter is devoted to the effects of data sampling rate on the convergence of the filtering scheme used. In each of these sections, results of computer simulations made in conjunction with the different model discussed will also be presented.

A. Single Satellite in a Plane

We shall ease into the relative positioning geodesy problem by first considering a simple example with planar geometry and a one-dimensional position uncertainty (Figure 4.1). In this tutorial

example, the distance between two points, one of which is a known reference, is to be determined from the satellite-receiver geometry by establishing the delay in time-of-arrival of the GPS signal wavefront at the two receiver locations. Proximity of the two points is further assumed such that the paths of incidence of the GPS signals to both points are ideally parallel. This negates the Doppler effect and elaborate geometries are thereby avoided.

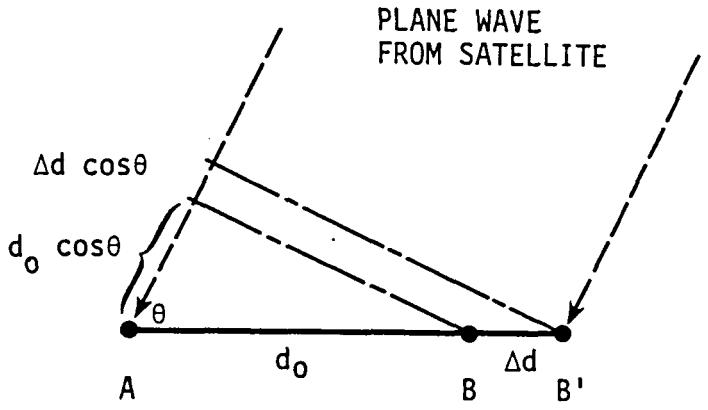

Figure 4.1. Single-satellite geometry for the one-dimensional incremental model

In Figure 4.1, Point A represents the reference. Using differential GPS techniques (normal navigation modes), a baseline A-B may be established accurate to within a few meters of the correct value. If B' is the actual location of the second point, we can then treat B-B' as an incremental perturbation. It is the determination of this incremental quantity that we will serve to address hereinafter.

In order to achieve this "fine-tuning" in accuracy, timing on the carrier phase of the GPS signal instead of the coded modulation (known in GPS terminology as the C/A and the P codes) is adopted. Assuming a phase-tracking rms error of 1/18 of a cycle, positional error, based on the 20-cm wavelength (approx.) GPS carrier, in the order of centimeters is feasible. This method, however, poses an inherent problem when tracking two phase-delayed signals, namely the ability to account for accumulated full cycles which is commonly referred to as the integer wavelength ambiguity problem for obvious reasons.

Going back to Figure 4.1 to formulate the problem, the relationship between the incremental phase and the incremental position is

$$\Delta\phi = \frac{\Delta d}{\lambda} \cos\,\theta(t) + \text{measurement noise} \qquad (4.1)$$

The increment in phase delay, $\Delta\phi$, can be considered as the difference between the total delay over A-B' and the delay over the nominal baseline A-B. As pointed out earlier, a phase delay carries an integer part (the accumulated full cycles) and a fractional one, of which only the latter can be electronically measured initially. Grouping the fractional terms together, we can rewrite eq. 4.1 as

$$\phi(\text{Mod1}) - \phi_0(\text{Mod1}) = (N-N_0) + \frac{\Delta d}{\lambda} \cos\,\theta(t) + \text{noise} \qquad (4.2)$$

Thus, the measurement model of eq. 4.2 and the process stated in the discrete form of eqs. 2.1 and 2.2 become

$$z_k = N' + x_k \cos\,\theta(t_k) + v_k \quad , \qquad N'=N-N_0 \qquad (4.3)$$

$$x_{k+1} = x_k \qquad (4.4)$$

where N and N_0 are the integer portions of the A-B' and A-B baseline phase delays initially. Modl denotes modulo 1 or a fraction of a cycle. All quantities related to the nominal assumption are known and will be tagged with the subscript 0. Note that eq. 4.2 is in the same form as the measurement model of eq. 2.2 with the quantity $(N-N_0)$ treated as an additive bias. In this formulation, $\Delta d/\lambda$ is the state variable of the process and the directional cosine term provides the linear connection between the state and the measurement, $(\phi-\phi_0)$. Also, note from eq. 4.4 that the state transition for a constant state is unity.

We now turn to the multiple hypothesis testing scheme, earlier discussed in the last section of the previous chapter, to resolve the unknown bias quantity $(N-N_0)$. However, while the earlier discussion dealt with a scheme that processed measurements containing the unknown additive bias, the measurements associated with our incremental GPS model here do not "include" the additive bias that has to be determined. The saving feature lies in the time-varying nature of the directional cosine term. It provides the necessary information on how the dynamics of the orbiting satellite will affect the variations in the phase measurements over a period of time. This allows the hypotheses to weed through the chaotic measurement noise and resolve out the true value of $(N-N_0)$.

The adaptive filter scheme was tested on a computer using simulated phase measurements that were generated from the same geometry described above for this single satellite scenario. Properly-scaled random numbers were used to represent the additive Gaussian white noise appearing also in the measurements. The parallel bank was set up to model eleven

hypotheses, consecutive integers from -5 to +5 (see Appendix B for program). The principal parameters used include:

Initial satellite trajectory angle = 30 degrees from horizon;

Angular rate of travel of satellite = 30 degrees per hour;

Data sampling interval = 20 seconds;

RMS of measurement noise (Gaussian) = 1/18 cycle;

Actual value of incremental position = 2.5 wavelengths; and

True value of integer ambiguity = -2.

The results shown in Figure 4.2 depict the progression of the weight factors $p(\alpha_i | z_k^*)$ as the discrete measurement data are processed. The set of 50 measurements represents an equivalent in a real-time acquisition interval of 1000 seconds or 16 2/3 minutes. In the interest of graphic clarity, only five of the parameters from the eleven filter elements were plotted. It is evident that the initialization influenced the zeroth filter to start off strongly ahead of the others. The eventual outcome from the tangled clutter saw the true filter modeled around the -2 integer clearly converge to unity after about 40 steps.

During the processing of the measurements, while the adaptive scheme was resolving the integer ambiguity, the filter that was modeled around the true integer -2 was also at the same time working its way towards an accurate estimate of the incremental position perturbation. Note from Figure 4.3 showing position estimates from 3 of the 11 filters that it did not take very long for the estimate of the true filter to converge to its actual value of 2.5 wavelengths.

Although the simulation presented above is but one sample run,

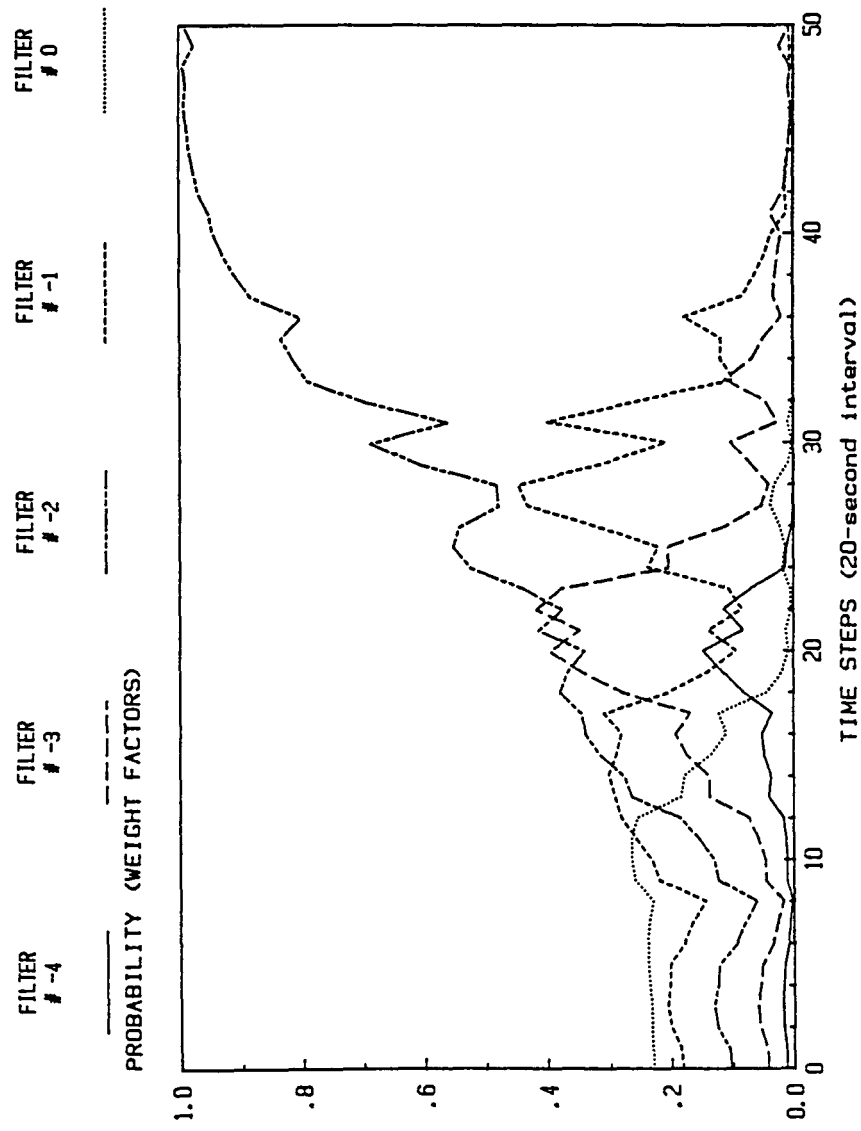

Figure 4.2. Plots of a posteriori probabilities from the one-dimensional single satellite example

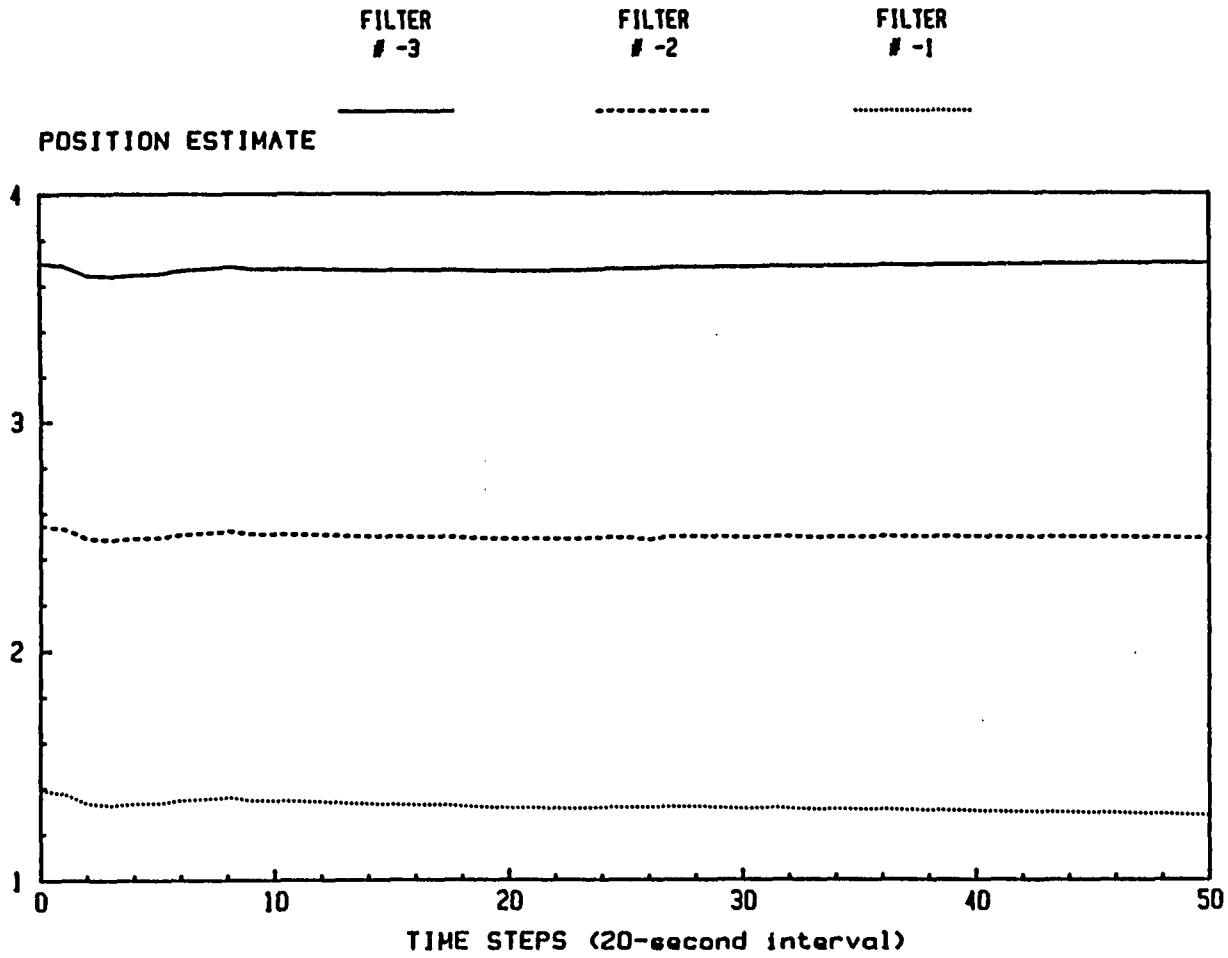

Figure 4.3. Plots of the state estimates of different filters from the one-dimensional single satellite example

results seen from others made with different sets of random numbers have been similar enough to consider this particular run only typical. No special numerical problems were encountered even though the complete form of the Magill algorithm given by eqs. 2.7 and 2.8 was implemented.

B. Accounting for Clock Error

In order to establish the phase delay of a GPS signal wavefront at two separate receiver locations, the ability to time the carrier phase of the GPS signal with precision using a local clock reference seems to be a crucial requirement imposed on the receiver equipment. It will become apparent later on in this section, though, that this clock error can be eliminated by redefining the measurement quantities. Before arriving at that, a major portion of this section will be devoted to the results obtained using the model from the previous section extended to include the clock error. Although this subject is now antiquated, it is nonetheless essential for the sake of completeness with regard to documenting the evolvement of this project.

When the phase of the carrier is measured at both receivers, it is timed relative to the local reference. Now since it is the difference in these two phase measurements that makes up the one measurement defined in our model, we can likewise consider a clock error to incorporate in our model as the difference in the errors of the local references of the two receivers. This error manifests itself in the measurement model as an additive zero-mean random variable and in the process as an appended state variable. The new model then becomes

$$x = [x_1 \quad x_2]^T \tag{4.5}$$

where:

$$x_1 = \frac{\Delta d}{\lambda}$$

$$x_2 = \varepsilon \qquad \text{(clock error)}$$

and,

$$z_i = [\cos \theta_i(t) \quad 1]x + v_i \quad ; \; i=1,2 \tag{4.6}$$

Because of the increase in the dimensionality of the state, a corresponding increase in the dimensionality of the measurement vector is required. The second measurement is obtained from another satellite with a different ephemeris. For our simplified example, we will stay with the planar geometry as in the previous section and keep this second satellite in the same plane sharing the trajectory of the first satellite. The hypothesis space (integer ambiguity) is now two-dimensional as well, that is, the parallel bank may be thought of as an array of filter elements laid out at the intersections of a grid.

To simplify the processing of the measurements somewhat, we can draw upon the assumption that the white noise terms appearing in both measurements are uncorrelated. Hence, sequential processing becomes an available option [6] and although it is not very clear that the computational savings are all that significant, this technique was adopted in all subsequent multi-dimensional problems simulated.

In a simulation using the process of eqs. 4.5 and 4.6, the geometric model of the earlier simulation was retained with the addition of a second satellite initially located on the circular trajectory 50 degrees from the horizon. The satellite is expectedly also traveling at equal

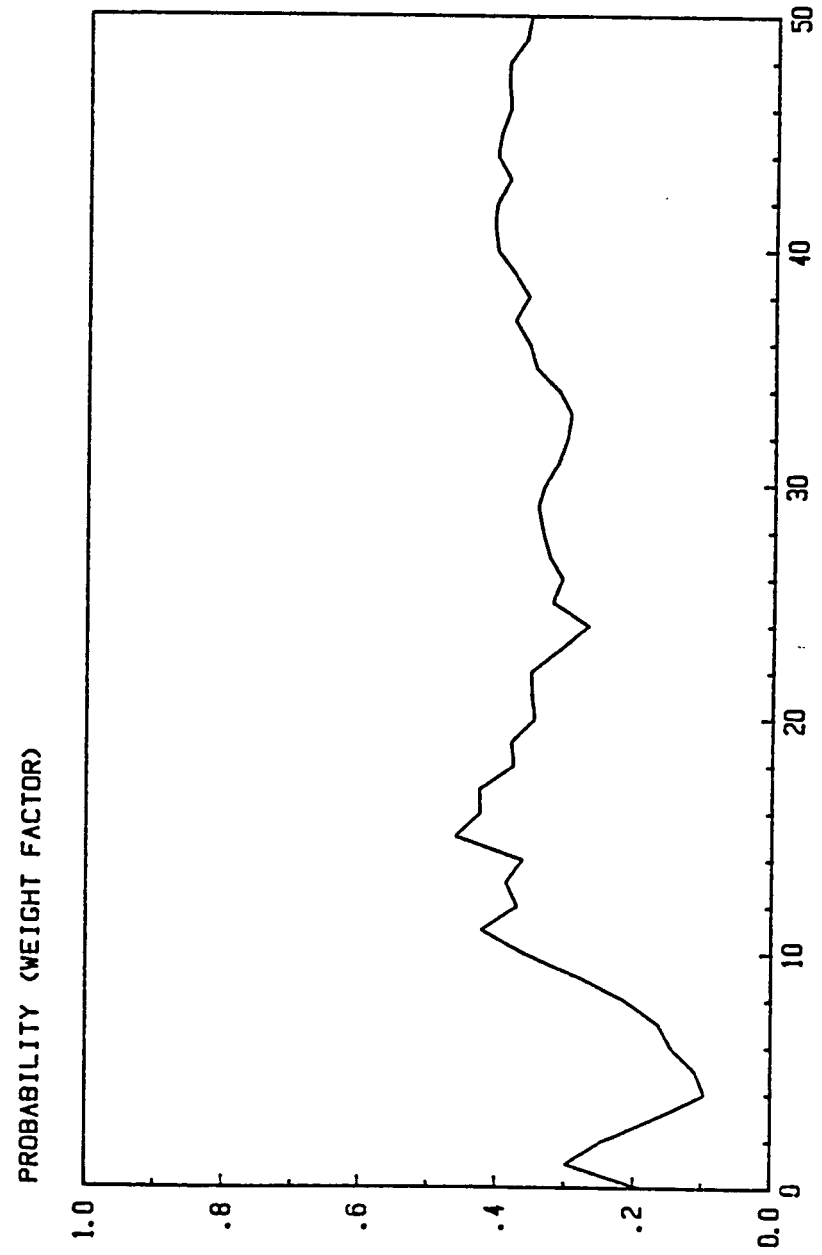

Figure 4.4. Plot of the a posteriori probability of the "true" filter from the one-dimensional 2-satellite model with clock error

rates and in the same orbital direction as the first one. Focusing our attention again on the weighting factor of the true filter in the array, the plot in Figure 4.4 shows a definite convergence after less than 20 steps, but the limit unlike before is not unity. It turned out that several other filter elements all belonging to the same "diagonal" of the 2-dimensional array also reached the same inconclusive state.

The reason for this condition is very simply that the clock error is unobservable. Without going into much detail, an intuitive explanation can be derived from the fact that while the directional cosine term connecting the position state variable to the measurement possesses that previously noted time-varying feature to resolve out the integer ambiguity, the same is not true of the linear connection (unity) for the clock error state variable. As a result, all the filters in that diagonal containing the true filter provided the same estimate for the position state while the estimates for the clock error state differed by one unit between adjacent filters. This, then, suggested that some combinatorial manipulation could be done to transform the scheme to eliminate the inestimable clock error and yet still account for it in the model.

A differencing technique which takes the difference of the two measurements, z_1 and z_2, and redefines it as a new measurement was then implemented. This differencing when incorporated into the measurement model gives (recall ε is the clock error):

$$z_1 - z_2 \triangleq (\cos\theta_1(t)\, x + (N-N_0)_1 + v_1 + \varepsilon) - (\cos\theta_2(t)\, x + (N-N_0)_2 + v_2 + \varepsilon)$$
$$= [\cos\theta_1(t) - \cos\theta_2(t)]x + N'' + v' \qquad (4.7)$$

The form of eq. 4.7 degenerates into that similar to eq. 4.3. In so doing, the variance of the newly-defined v' is now twice that of the original v. Fortunately too, the dimensionality of the state is reduced by one, a benefit that will prove significant especially when dealing with higher-order geometries such as one encountered in the next section.

C. Three-Dimensional Geometry

As an extension from the "satellites-in-a-plane" geometry, the number of satellites required to solve the 3-space perturbation problem with inclusion of clock error now becomes four. This would expand the hypothesis space of the Magill adaptive scheme to one with four dimensions. The differencing technique introduced in the previous section to eliminate the clock error in turn reduces the dimensionality to three. This constitutes a huge savings in terms of the number of filter elements required ($n^3 << n^4$ if n is large).

The geometry of the satellite trajectories was set up to imitate the real-life GPS model. Figure 4.5 depicts the orbital rings from a visual orientation looking down on the North Pole. The 3 rings, of which only 2 are shown, are spaced 120 degrees apart and the planes of the rings are inclined 30 degrees from the polar plane. Satellites belonging to the same orbit are separated by 60 degrees of arc. In addition to this, a rotation of the entire structure about the polar axis was included to

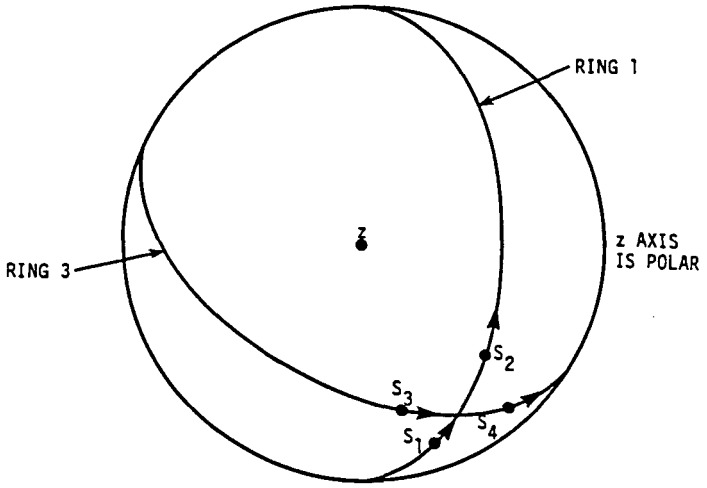

Figure 4.5. Geocentric satellite geometry for the 3-dimensional 4 satellite model (Z-axis is pointing out of the page)

investigate the possible influence of the rotating earth.

The positions of the four satellites were chosen such that they remained fairly closely clustered over the observation time interval to ensure visibility of all the satellites as they are viewed from an appropriate location on the surface of the earth. As far as the measurement model was concerned, it was assumed that the observations were made in geocentric (center-of-the-earth) coordinates, which, in other words, placed the observation point right in the center of the spherical model of Figure 4.5. Although this seems somewhat detached from reality, the truth of the matter is that the observation point can readily be transferred to the surface of the earth through a coordinate transformation which would, at this point, unnecessarily clutter up the computations with excessive algebra. In any case, we are assured that any distortion

arising from this simplification would yield results that are more pessimistic than the actual because an improvement in the Geometric Dilution of Precision (GDOP) factor (refer to Chapter III for a definition of this term) can otherwise be obtained. Figure 4.6 sufficiently clarifies this point using a planar analogy.

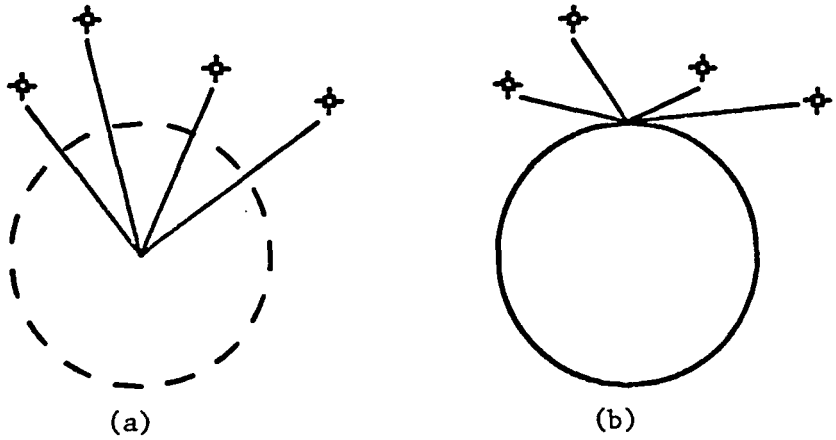

Figure 4.6. For the same satellite distribution, a geocentric-coordinate model (a) yields higher GDOP than a geodetic one (b)

In formulating the measurement model for the 3-dimensional geometry, we will use only generalized representations for the directional vectors. The equation for the "raw" measurements obtained from the satellites can be written, as before,

$$\Delta\phi_i = D_i \cdot x + N_i' + \varepsilon + v_i \; ; \qquad i=1,2,3,4 \tag{4.8}$$

where:

$$E[v_j v_k] = 0 \ , \ j \neq k$$
$$= (1/18)^2 \ , \ j=k$$

The operator $E[\cdot]$ denotes the average or expected value. Also, D_i is the direction cosine row vector for the ith satellite and x, the state vector representing the 3-space perturbations in earth-fixed X, Y, Z Cartesian coordinates. Using the following differencing scheme,

$$\begin{aligned} z_1' &= \Delta\phi_1 - \Delta\phi_2 \\ z_2' &= \Delta\phi_3 - \Delta\phi_4 \\ z_3' &= (\Delta\phi_1 + \Delta\phi_2) - (\Delta\phi_3 + \Delta\phi_4) \end{aligned} \tag{4.9}$$

or

$$z_i' = D_i' \cdot x + N_i'' + v_i' \ ; \quad i=1,2,3$$

it can be shown that the newly-defined measurements z_1', z_2', and z_3' are statistically independent. We consider,

$$\begin{aligned} E[v_1' v_2'] &= E[(v_1 - v_2)(v_3 - v_4)] \\ &= E[v_1 v_3 - v_1 v_4 - v_2 v_3 + v_2 v_4] \\ &= 0 \end{aligned}$$

$$\begin{aligned} E[v_1' v_3'] &= E[(v_1 - v_2)(v_1 + v_2 - v_3 - v_4)] \\ &= E[v_1 v_1 + v_1 v_2 - v_1 v_3 - v_1 v_4 - v_2 v_1 - v_2 v_2 + v_2 v_3 + v_2 v_4] \\ &= E[v_1 v_1] - E[v_2 v_2] \\ &= 0 \end{aligned}$$

Similarly,

$$E[v_2'v_3'] = E[(v_3-v_4)(v_1+v_2-v_3-v_4)]$$
$$= -E[v_3v_3] + E[v_4v_4]$$
$$= 0$$

This scheme was adopted to ensure retention of the use of sequential processing in the computational scheme. Here again, as before, the variances of the redefined associated noise terms are increased accordingly:

$$E[v_1'v_1'] = E[v_2'v_2'] = 2\ (1/18)^2$$
$$E[v_3'v_3'] = 4\ (1/18)^2$$

In a simulation run where the now expanded version of the adaptive filter scheme was tested using the new simulated geometry, the results obtained were very encouraging. The filter structure is now three-dimensional and, in retaining the integer ambiguity range of -5 to +5, the number of filter elements implemented was 11^3 or 1331, a staggering figure for the rather limited range of coverage. Figure 4.7 displays results gathered from three typical simulation runs made. Again, the weighting factor $p(\alpha_i | z_k^*)$ of the true filter is plotted against the measurement time steps, fifty in all, representing 1000 seconds of actual observation time. Also, the progression of the state variables in the estimate vector of the true filter through the entire recursion is summarized in Table 1. The actual perturbations in the X, Y, Z directions incorporated in the problem were $x = [1.5 \quad 1.5 \quad 1.5]^T$.

A notable presence in the results (Table 1) featured is the sluggish

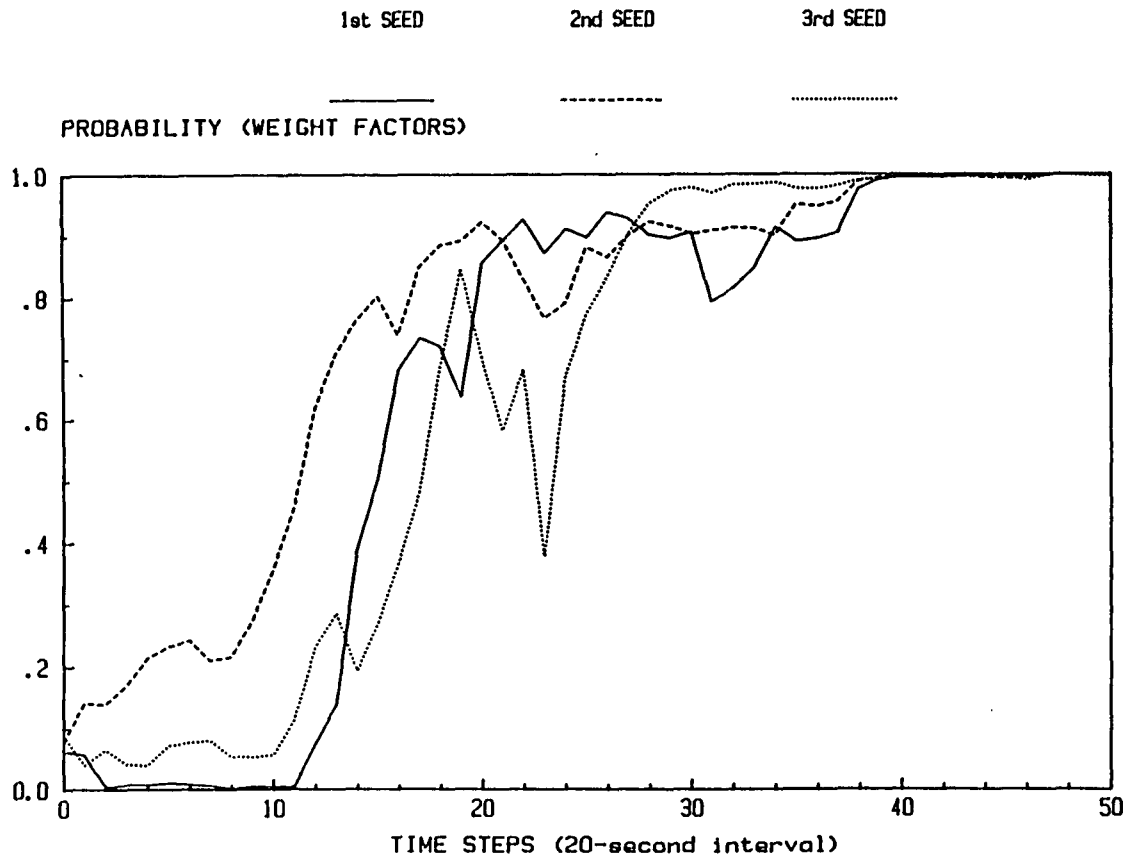

Figure 4.7. Plot of a posteriori probability of the "true" filter for 3 typical runs of the 3-dimensional 4 satellite model

Table 1. Computer listing of the state estimate vector and the a posteriori probability of the "true" filter in the simulation of the 3-dimensional 4 satellite model

STEP	X(TRUE)	Y(TRUE)	Z(TRUE)	PROB(TRUE)
0	0.445	1.179	0.579	0.062
1	0.824	1.298	0.968	0.056
2	2.105	1.641	2.228	0.004
3	2.376	1.685	2.449	0.008
4	2.147	1.661	2.226	0.008
5	1.508	1.522	1.585	0.011
6	0.894	1.380	0.958	0.008
7	0.590	1.290	0.647	0.006
8	0.126	1.170	0.170	0.001
9	0.265	1.202	0.316	0.005
10	0.342	1.215	0.384	0.004
11	0.357	1.224	0.373	0.005
12	0.480	1.262	0.511	0.075
13	0.458	1.257	0.492	0.139
14	0.956	1.385	0.992	0.389
15	1.081	1.412	1.125	0.503
16	1.090	1.418	1.129	0.682
17	1.335	1.481	1.378	0.734
18	1.767	1.596	1.816	0.720
19	1.611	1.551	1.660	0.637
20	1.635	1.560	1.678	0.856
21	1.698	1.580	1.740	0.893
22	1.577	1.547	1.610	0.926
23	1.769	1.601	1.801	0.872
24	1.684	1.578	1.711	0.910
25	1.728	1.589	1.754	0.897
26	1.634	1.562	1.658	0.938
27	1.746	1.594	1.776	0.928
28	1.816	1.615	1.842	0.901
29	1.858	1.627	1.886	0.896
30	1.881	1.634	1.911	0.907
31	2.001	1.671	2.030	0.794
32	1.971	1.663	1.995	0.815
33	1.945	1.654	1.968	0.847
34	1.774	1.603	1.791	0.914
35	1.830	1.620	1.851	0.892
36	1.841	1.624	1.858	0.896
37	1.812	1.615	1.829	0.906
38	1.762	1.599	1.777	0.977
39	1.689	1.576	1.702	0.993
40	1.717	1.585	1.731	0.996
41	1.727	1.588	1.742	0.995
42	1.674	1.572	1.681	0.995
43	1.646	1.563	1.649	0.998
44	1.610	1.551	1.614	0.998
45	1.605	1.550	1.610	0.999
46	1.528	1.525	1.528	0.998
47	1.605	1.550	1.613	1.000
48	1.623	1.555	1.630	1.000
49	1.541	1.528	1.546	1.000
50	1.566	1.536	1.574	1.000

convergence of the X- and Z-components of the state vector for the true filter. The principal reason for this lies in the geometry which yields, as mentioned before, poor GDOP characteristics. This manifests itself in causing the determinant of the measurement matrix (the linear connection between the state and the measurement vectors) to be small in magnitude. Using this to be a measure of the "degree of observability," the choice of satellites, should the luxury of sighting more than four be afforded, may then be based on the maximization of this parameter.

The plots of Figure 4.7, on the other hand, show little effect that the poor geometry might have had on the convergence of the adaptive estimator if any at all. Comparing them to the example of the single satellite case in the first section, the time it takes to converge to unity is reasonably similar in all cases, about 13 to 15 minutes of observation time. It would seem reasonable to deduce, then, that while the spatial dimensionality has increased three-fold in this problem, the amount of information harnessed from enlisting the involvement of the additional satellites has correspondingly increased as well.

D. Effects of Increased Sampling Rates

The cause which prompted investigation into this area was the slow convergence of the state and its associated error covariance due to poor geometry as encountered in the 3-dimensional problem of the previous section. Several other parameters apart from the measurement matrix play a role in the convergence of the Kalman filter (different from the convergence of the Magill adaptive filter), one of which is the data sampling rate. Since the random process considered here is constant,

there is no input process noise involved in the model of eq. 4.4. While it is often unwise to model a process strictly as a stationary random bias [6], the relatively short observation spans involved reduce the risk of divergence. The limit of convergence of the error covariance in this case is then zero.

Now if the sampling rate is increased so that the measurement sequence is lengthened for the same observation time span, the filter will invariably yield a better estimate after processing all the data collected. Through simulation runs similar to those of the earlier sections, but made with increased sampling rates, it was discovered that in addition to confirming the above, the rate of convergence of the adaptive scheme in locating the true filter, in a real time sense, is also improved.

Due to the greater processing effort involved in simulating models with high sampling rates (greater amounts of data), studies in this area were restricted to the simplified one-dimensional case from the first section of this chapter. The results of three separate runs made with varying sampling rates are summarized in Figure 4.8, showing the weight factor of the true filter plotted against the real time equivalent of the measurement data processed. It is apparent that the increase in the convergence rate is not linearly proportional to an increase in the sampling rate.

While it may seem that the overall performance of the Magill adaptive scheme is benefited by a faster sampling rate, it must be considered that there are physical limitations that can hinder such an

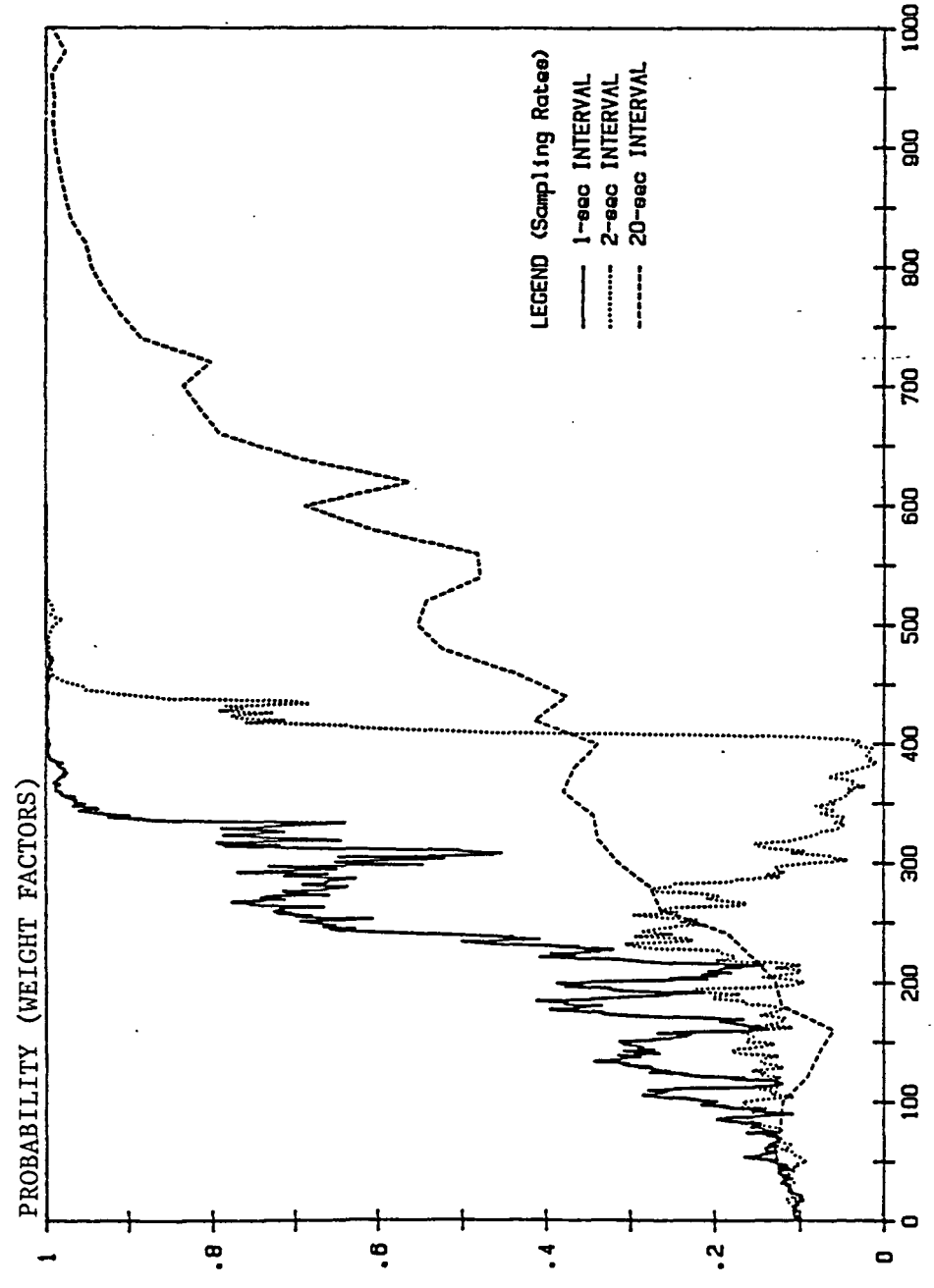

Figure 4.8. Plots of the a posterior probability of the "true" filter from the one-dimensional single satellite example using different sampling rates

implementation. If the sampling rate is too high, the data acquisition requirements will consequently become extremely stringent as well. This is also true of processing requirements should the implementation be one of real-time. A more severe systems limitation manifests itself in the degree of correlation among the discrete samples since it increases with a diminishing sampling time interval. Since the Kalman filter formulation adopted makes the assumption that all such discrete samples must remain uncorrelated, the optimality of the filter, therefore, hinges upon the degree of "uncorrelatedness" of the samples.

V. COMPUTATIONAL CONSIDERATIONS FOR LARGE INTEGER AMBIGUITY IMPLEMENTATIONS

In the 3-dimensional example of the last chapter, the range of integer ambiguity was restricted to 11 units in each of 3 dimensions. Even with this very limited range, it was necessary to run over a thousand Kalman filters in parallel. Clearly, this can get out of hand in cases where the integer ambiguity is large. In the actual GPS application, for instance, it might be more realistic to consider an uncertainty in the order of 100 per dimension, in which a million Kalman filters would be required should the Magill scheme be implemented literally as was done earlier.

Fortunately, it was found that a deterministic relationship exists among the filter elements of the parallel bank. It will be seen later on that this relationship is monotonic in nature, hence allowing us to regard the hypothesis space as a continuum rather than as a "bank of discrete filters." Similarly, the unknown integer vector (a 3-tuple) can be treated as a continuous random variable amenable to estimation by either maximum likelihood (as we have been doing with the Magill adaptive scheme), or Bayesian (Kalman filtering) methods.

In this chapter, we will address the maximum likelihood method first as it constitutes a generalization of our discrete formulations up to this point. In a separate section, we will look at the Kalman filtering alternative in estimating this unknown integer vector. For reasons of relevance, we will in this chapter refrain from reference to "the true filter" as before in the discrete sense and instead use the reference

of the "correct hypothesis" to mean the same.

A. Maximum Likelihood

The concepts presented in this section are no more than generalizations from those in the last chapter except that the descriptions will often revolve around the notions of a continuous hypothesis space unlike before. The deterministic relationship found to exist among the filter elements had suggested that there was no need to numerically keep track of all the filter parameters in each and every element in the parallel structure. Rather, a knowledge of the relationship or function that tied them together was sufficient to propagate through each cycling of the Kalman filter algorithm. This essentially reduced the "bank" to the processing of one filter modified to accommodate this idea.

To introduce the notation used, x represents as before the state vector, and u, the hypothesis (or parameter) vector as defined by the Magill adaptive scheme. If we consider that x is a linear function of u, then we can write

$$x = [C \quad b]u_a \tag{5.1}$$

where C is the coefficient matrix of u and it is augmented with the constant vector b; also, $u_a = [u \quad 1]^T$. The measurement residual is then given by

$$r_k(u_a) = y_k(u_a) - H_k[C_k \quad b_k]u_a \tag{5.2}$$

recalling that y, the "processed measurement" (obtained after the raw

measurement has been "adjusted by the hypothesized" amount in the equivalent discrete case), is a linear function of the hypothesis. The Kalman filter state update and projection equations of eq. 2.4 and eq. 2.6b now become

$$\hat{x}_k^+(u_a) = \hat{x}_k^-(u_a) + K_k r_k(u_a) \tag{5.3a}$$

$$\hat{x}_{k+1}^-(u_a) = \hat{x}_k^+(u_a) \tag{5.3b}$$

where K, the Kalman gain, is constant and independent of u. The Kalman gain and state error covariance which make up the rest of the filter algorithm are computed as usual without any modifications.

At the start of the filtering process, the initial a priori estimate of the state, $\hat{x}_0^-$ in all the filter elements is set equal to a constant vector which, in this scheme, makes up b. Now, the recursive nature of eq. 5.3 then implies that once the filter is "started up" with a vector $\hat{x}_0^-$ linear in u, then $\hat{x}_k^+$, and hence r_k, will remain linear in u for all t_k thereafter.

Next, we consider a modified form of the log-likelihood function taken from eq. 2.9:

$$\begin{aligned} L_k(u_a) &\triangleq 2 \log_e p(z_k^* | u_a) \\ &= - \sum_{j=0}^{k} r_j^T(u_a) V_j^{-1} r_j(u_a) \end{aligned} \tag{5.4}$$

where V_j is the error covariance associated with the jth measurement residual. Drawing from the fact that the sum of quadratic functions is itself quadratic, eq. 5.4, then, is of the form

$$L_k(u_a) = u_a^T W_k u_a \tag{5.5}$$

When this is maximized with respect to u_a (the actual value of $L(u_a)$ at the maximum is not important here), we obtain

$$\frac{d}{du_a} L_k(u_a) = 2 W_k u_a \tag{5.6}$$

$$W_k u_a \triangleq \begin{bmatrix} w_{11} & w_{12} & w_{13} & w_{14} \\ w_{21} & w_{22} & w_{23} & w_{24} \\ w_{31} & w_{32} & w_{33} & w_{34} \\ w_{41} & w_{42} & w_{43} & w_{44} \end{bmatrix}_k \begin{bmatrix} u_1 \\ u_2 \\ u_3 \\ 1 \end{bmatrix}$$

Hence, setting $W_k u_a = 0$ yields the location of the maximum, $\hat{u}_k^*$:

$$\hat{u}_k^* = \begin{bmatrix} \hat{u}_1^* \\ \hat{u}_2^* \\ \hat{u}_3^* \end{bmatrix} = - \begin{bmatrix} w_{11} & w_{12} & w_{13} \\ w_{21} & w_{22} & w_{23} \\ w_{31} & w_{32} & w_{33} \end{bmatrix}_k^{-1} \begin{bmatrix} w_{14} \\ w_{24} \\ w_{34} \end{bmatrix} \tag{5.7}$$

$\hat{u}_k^*$ need only be computed as required since it is not a parameter essential to the recursion of the process. The circumflex on $\hat{u}_k^*$ is used to indicate that the quantity is an estimate of the random variable u_k^* and, depending on the influence of the initial a priori conditions set for the filters as well as that of the noise in the measurement sequence, it will gradually converge, in a statistical sense, on the correct hypothesis. When working with brief sequences of measurement data though, $\hat{u}_k^*$ will in all likelihood end up being anywhere but at an

"integer" location which is a strict requirement built into our original model. Reverting to a geometric viewpoint of the three-dimensional bank of filter elements, the "integer" location referred to is one of the discrete intersections of the grid structure meshed one unit apart. Our goal remains then to find the discrete "integer" location that carries the largest value of the likelihood function. Using eq. 5.5, we can compute the values of the log-likelihood for the vertices of a unit cube geometrically containing $\hat{u}_k^*$, the vertices being at "integer" locations. The vertex having the largest value of the comparison of the eight points is then taken to be the location of the correct hypothesis, the coordinates of which, when substituted back into a relationship similar to eq. 5.1 for t_k, yield the state estimate vector $\hat{x}_k$.

As an example, we consider a one-state process where the notation follows from before:

Step 0: $$\bar{x_0} = [C_0 \quad b_0]\begin{bmatrix} u \\ 1 \end{bmatrix}$$

(Since $\hat{\bar{x}}_0$ is always set to be the same for all filters in a parallel adaptive arrangement, and is usually set equal to zero if a zero-mean distribution is assumed, then $C_0 = b_0 = 0$.)

$$y_0 = z_0 - u$$

(z_0 is the raw measurement at t_0.) Computing the residual from eq. 5.2,

$$r_0 = \begin{bmatrix}-1 & z_0\end{bmatrix}\begin{bmatrix}u\\1\end{bmatrix} - H_0\begin{bmatrix}C_0 & b_0\end{bmatrix}\begin{bmatrix}u\\1\end{bmatrix}$$

$$= \begin{bmatrix}-(1+H_0C_0) & (z_0-H_0b_0)\end{bmatrix}\begin{bmatrix}u\\1\end{bmatrix}$$

$$\triangleq \begin{bmatrix}s_0 & t_0\end{bmatrix}\begin{bmatrix}u\\1\end{bmatrix}$$

Updating the state estimate as in eq. 5.3,

$$\hat{x}_0^+ = \begin{bmatrix}C_0-K_0(1+H_0C_0) & b_0+K_0(z_0-H_0b_0)\end{bmatrix}\begin{bmatrix}u\\1\end{bmatrix}$$

$$\hat{x}_1^- = \hat{x}_0^+ \triangleq \begin{bmatrix}C_1 & b_1\end{bmatrix}\begin{bmatrix}u\\1\end{bmatrix}$$

Forming the log-likelihood function from eq. 5.4,

$$L_0 = \begin{bmatrix}u & 1\end{bmatrix}\begin{bmatrix}s_0^2/V_0 & s_0t_0/V_0\\ s_0t_0/V_0 & t_0^2/V_0\end{bmatrix}\begin{bmatrix}u\\1\end{bmatrix}$$

Step 1: Repeat as above for r_1 and $\hat{x}_1^+$. The log-likelihood function is then (see eq. 5.4),

$$L_1 = L_0 + \begin{bmatrix}u & 1\end{bmatrix}\begin{bmatrix}s_1^2/V_1 & s_1t_1/V_1\\ s_1t_1/V_1 & t_1^2/V_1\end{bmatrix}\begin{bmatrix}u\\1\end{bmatrix}$$

Step k: Locating the maximum of the log-likelihood function as in eqs. 5.5-5.7,

$$L_k = \begin{bmatrix}u & 1\end{bmatrix}\begin{bmatrix}w_{11} & w_{12}\\ w_{21} & w_{22}\end{bmatrix}\begin{bmatrix}u\\1\end{bmatrix}$$

$$\hat{u}_k^* = -\frac{w_{12}}{w_{11}}$$

This recursion is carried on until all the measurements available are processed. In implementing the above, only the linear connection matrices and, in the case of the log-likelihood function, the weighting matrix, need to be computed and carried through each cycle of the process.

The results of a simulation using the above scheme on the full 3-dimensional model are summarized in Figure 5.1. The unknown perturbations to be estimated were arbitrarily chosen to be $\Delta X = -46.1$, $\Delta Y = -35.3$, $\Delta Z = 70.8$, with the corresponding unknown integers being $u^* = [64\ -71\ 31]^T$. As before, the measurement sequence used consisted of 50 sets of measurements from four satellites sampled at 20-second intervals. u^* is shown plotted in each dimension against the measurement time steps (see Appendix for program).

In the unlikely event that the true element is located far away from the initial a priori assumption, the rate of convergence will deteriorate simply because there is an "increase" in the required effort to nullify the bad initial assumption. In such cases, the adaptive scheme may actually "home in" on the wrong location. Due to the convexity of the log-likelihood function, however, it is still possible to locate the true element by making several runs, each successive run using, as its initial state, the state estimate resulting from the previous run. This cycling is kept up until consecutive runs yield the same "true" element. Thus, a minimum of two cycles are required for the purpose of verification. Even if several runs are needed to obtain the solution, the processing time involved is truly minimal.

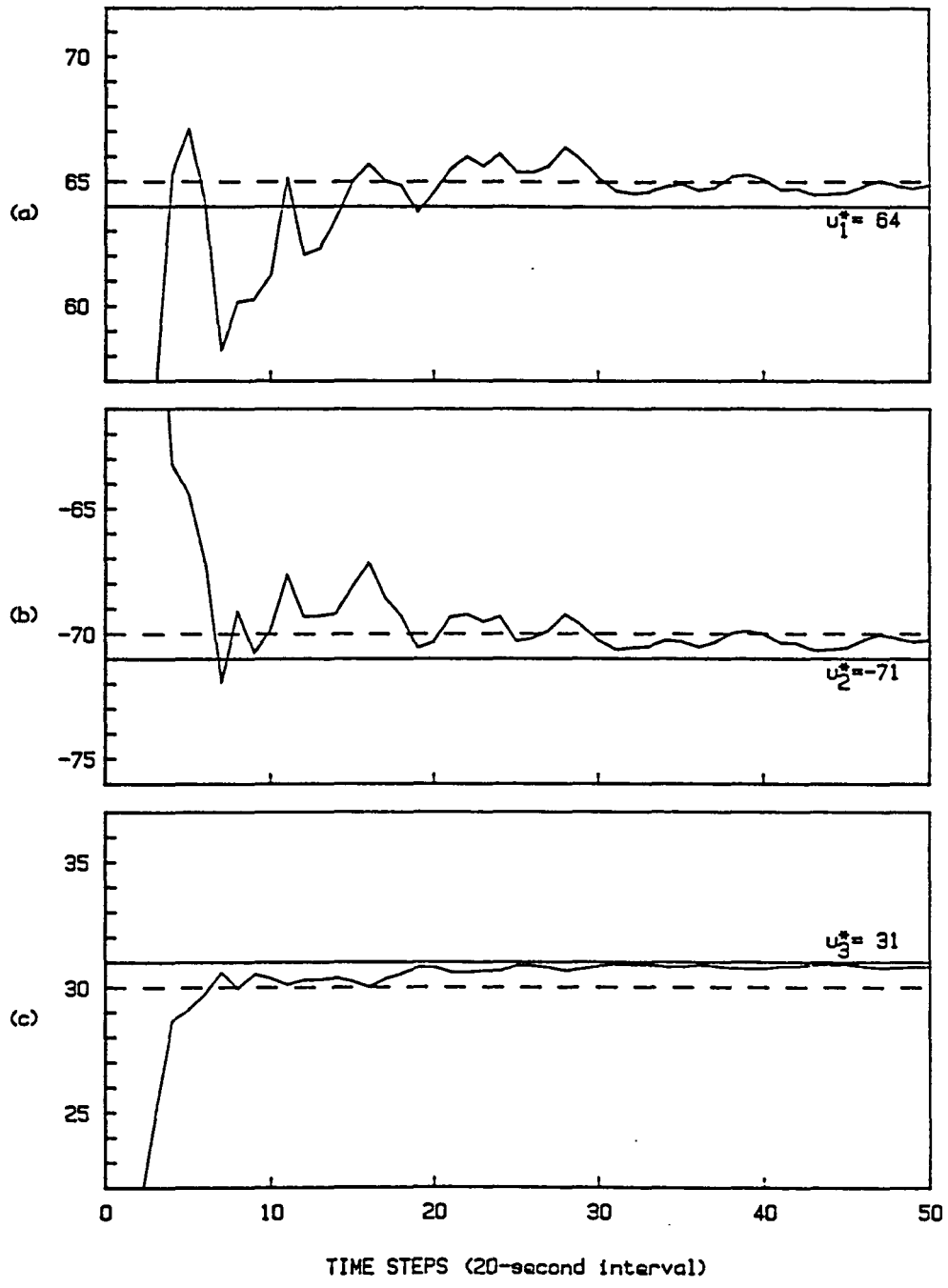

Figure 5.1. Plots of (a) $\hat{u}_1^*$, (b) $\hat{u}_2^*$, and (c) $\hat{u}_3^*$ show that each component converges to within one unit (dotted lines) of its actual value

B. The Augmented Kalman Filter

By treating the unknown integer vector as a continuous random variable, we therefore redefine the multiple hypothesis testing concept of solving for the integer ambiguity to be a problem in estimation. In so doing, the Kalman filter again becomes a viable option to accomplish the task. In rewriting the differenced measurement model of eq. 4.9 from the last chapter, we obtain

$$z_j' = D_j' \cdot x + N_j'' + v_j' \tag{5.8}$$

with the prime notation indicating newly-formed quantities from the differencing operation which eliminates the clock error. Now if the additive integer N_j'' were inducted into the state vector, henceforth creating a 6-tuple made up of the original "position" 3-tuple vector x and augmented with N_j'' (for j=1,2,3) representing the 3-tuple "hypothesis" vector, eq. 5.8 then becomes

$$\begin{bmatrix} z_1' \\ z_2' \\ z_3' \end{bmatrix} = \begin{bmatrix} D_{X1}' & D_{Y1}' & D_{Z1}' & 1 & 0 & 0 \\ D_{X2}' & D_{Y2}' & D_{Z2}' & 0 & 1 & 0 \\ D_{X3}' & D_{Y3}' & D_{Z3}' & 0 & 0 & 1 \end{bmatrix} \begin{bmatrix} X \\ Y \\ Z \\ N_1'' \\ N_2'' \\ N_3'' \end{bmatrix} + \begin{bmatrix} v_1' \\ v_2' \\ v_3' \end{bmatrix} \tag{5.9}$$

Here again, the process is considered to be a stationary random bias

with the trivial dynamics described by

$$[X \quad Y \quad Z \quad N_1'' \quad N_2'' \quad N_3'']^T_{k+1} = [X \quad Y \quad Z \quad N_1'' \quad N_2'' \quad N_3'']^T_k \qquad (5.10)$$

In the initialization of the filter, the "startup" a priori values associated with the "hypothesis" part of the state is constrained by those specified for the original "position" portion because, as shown previously, the two elemental vectors are linearly, and hence uniquely related. To formulate the initial state of the filter, we will digress to reexamine the one-dimensional two-satellite differenced measurement model of eq. 4.7,

$$z' = z_1 - z_2 = h \cdot x + N'' + v' \qquad (5.11)$$

where:

$$h = [\cos \theta_1(t) - \cos \theta_2(t)]$$

The "raw" measurements, z_1 and z_2, at time t_0, being measurable only as a fraction of a cycle, can be assigned a uniform distribution over the internal of 0 to 1. The resulting distribution of z', the difference of two uniform distributions, then is triangular in form and symmetric (from -1 to +1) about zero. Hence, the random variable z' is zero-mean and has a variance of 1/6.

Eq. 5.11 remains unbiased and thus, the initial a priori state vector can be set to the null vector. To compute the initial a priori error covariance matrix $\bar{P_0}$, the variance of the first stage variable must be specified; let it be q. The remaining terms in the matrix may now be

readily computed given q. Rewriting eq. 5.11 in terms of N'' and computing its variance (Var) while ignoring v',

$$N'' \cong -x \cdot h + z'$$

$$\begin{aligned} \mathrm{Var}(N'') &= \mathrm{Var}(x \cdot h) + \mathrm{Var}(z') \\ &= h^2 q + 1/6 \end{aligned}$$

The variance of the measurement noise v is comparatively small and is as such neglected. For the cross-covariance (Cov) term,

$$\begin{aligned} \mathrm{Cov}(N'') &= E[(-x \cdot h)\, x] + E[z'] \\ &= -qh + 0 \end{aligned}$$

The notation $E[\cdot]$, as encountered before, denotes the average or expected value. The variables x and z' above are assumed to be uncorrelated for large values of x.

Therefore, with this measurement model, we start out the augmented Kalman filter with the initialization,

$$\bar{x}_0 = 0$$

$$\bar{P}_0 = \begin{bmatrix} q & -qh \\ -qh & h^2 q + 1/6 \end{bmatrix} \qquad (5.12)$$

As in the case of the maximum likelihood option, the augmented Kalman filter provides the means for a preliminary run to narrow down the uncertainty of the unknown integer so that when the discrete hypotheses of the Magill adaptive filter are ultimately reverted to, the scale of implementation involved becomes delightfully manageable.

In extending the above to the three-dimensional model and retaining the notation of eq. 5.9, the initial a priori state and its associated error covariance then become (see Appendix A):

$$[X \quad Y \quad Z \quad N_1'' \quad N_2'' \quad N_3'']^T = 0$$

$$P_0^- = \begin{bmatrix} P_x & -P_x H_0^T \\ -H_0 P_x^T & H_0 P_x H_0^T + F \end{bmatrix} \tag{5.13}$$

where:

$$F = \begin{bmatrix} 1/6 & 0 & 0 \\ 0 & 1/6 & 0 \\ 0 & 0 & 1/3 \end{bmatrix}$$

where P_x is a 3x3 covariance matrix specifying the 3-position error in the incremental perturbation from the nominal, and H_0, the 3x3 directional matrix providing the linear connection between the positive state variables, X, Y, Z and the 3-tuple measurement vector. The general procedure involved with the rest of the filter is essentially the same as already described for the one-dimensional example.

The results obtained using the augmented Kalman filter were predictably very similar to those obtained using the maximum likelihood approach given in the last section (see Appendix B for program). Analysis of the results and a brief comparative study of these two methods will be the topic of focus reserved for the last section of this chapter.

C. A Comparison of the Maximum Likelihood and the Augmented Kalman Filter Approaches

The comparative analysis to be presented in this section will concentrate only on results obtained on the one-dimensional two-satellite differenced measurement model with planar geometry. This simplified example serves to present a picture free of clutter from algebraic details and yet not suffer any loss of generality since extension to its 3-dimensional counterpart is readily accomplished.

The results obtained with the augmented Kalman filter from processing computer-simulated measurements show a similarity in the steady-state with those obtained using the maximum likelihood scheme. This, then, suggested that with the appropriation initialization of the Kalman filter, results as those of the maximum likelihood version could be duplicated. Figure 5.2a shows the effect on the results for the augmented Kalman filter of varying the values in the 2,2-entry of the error covariance matrix in eq. 5.12. This parameter corresponds to the initially-assumed variance of the unknown integer vector. The graph depicts the deviation, from the "optimal" version, of the unknown integer estimates, the latter obtained using the augmented Kalman filter initialized with eq. 5.12. The same noisy measurement data sequence was used in all cases for the comparative purpose of eliminating the random nature of the stochastic process. The smooth curves plotted against the measurement time steps clearly indicate that the maximum likelihood (Figure 5.2b) and the augmented Kalman filter schemes coincide in the steady-state. In addition, they also show that the maximum likelihood scheme

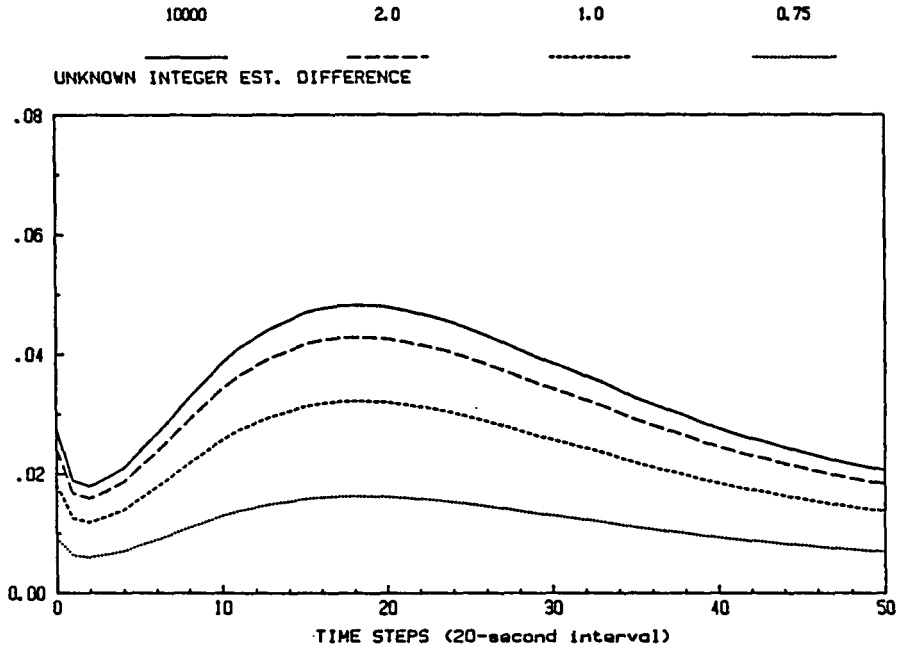

(a)

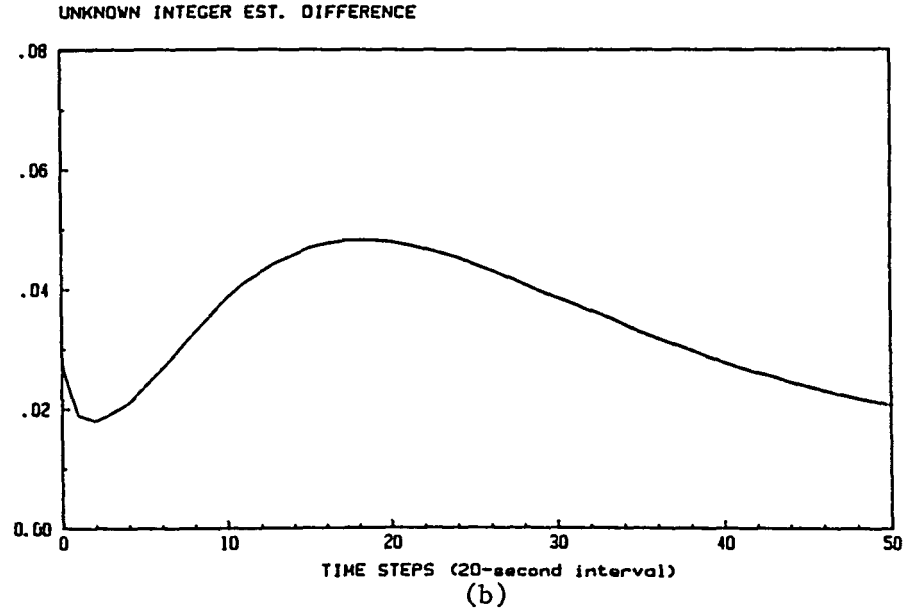

(b)

Figure 5.2. The augmented Kalman filter (a) coincides with the maximum likelihood method (b) when the initially-assumed variance of the unknown integer gets very large

is the limiting case of the augmented Kalman filter when the initially-assumed variance of the unknown integer vector is allowed to become very large.

Qualitatively, this means that the maximum likelihood scheme concedes to having no prior information whatsoever about the probability distribution of the integer ambiguity. This can additionally be verified from eq. 5.5 where the quadratic-form weighting matrix W_k is initialized as $W_0 = 0$, thereby taking on an even distribution which, in the Gaussian context, implies infinite variance. Although optimality can still be achieved by embedding the a priori information into this matrix, this is not a common practice in the use of the maximum likelihood technique and neither is it convenient to do so. In this respect, the augmented Kalman filter provides the optimal solution to the problem of estimating the integer ambiguity.

Also, in addition to this, the state error covariance matrix conveniently keeps track of the variance of this parameter as it cycles through the recursive algorithm of the Kalman filter. This parameter can be used as a confidence indicator of the estimate at hand, and the ease of computing it lends a benefit to the data acquisition process with regard to specifying the amount of data needed to meet a required confidence criterion.

Lastly, it is appropriate to comment on certain processing considerations marginally in favor of the maximum likelihood method. Comparing the dimensionality of the two approaches, it is obvious that the computational burden, however minimal, is lighter in the case of the 3-state

maximum likelihood scheme than the 6-state augmented Kalman filter. Also, in the maximum likelihood scheme, the transition from the preliminary estimation of the integer ambiguity to the "fine" estimation of the fractional phase is trivial since eqs. 5.1 and 5.5 readily yield the required quantities for the discrete Magill adaptive implementation.

VI. CONCLUSIONS

A. Summary of Results

The results obtained over the entire period of the study have shown that the Magill adaptive scheme possesses considerable promise in its application to the field of GPS geodesy. The results that have been presented can be summarized in three groups:

(a) Computer simulations of the incremental GPS model (Chapter IV):

The one-dimensional single satellite model with planar geometry demonstrated convergence in resolving the integer ambiguity in the range of 13 to 15 minutes of equivalent observation time. The estimation of the "true" fractional part of the phase itself converged in even less time.

(b) Simulations investigation the effects of varying the sampling rates Chapter IV):

Using the one-dimensional model again, the results from drastically increasing the data sampling rate showed a remarkable improvement in the convergence: 7-8 minutes for a 2-second sampling interval, and 5-6 minutes for a 1-second sampling interval. This gain is, of course, not without a price; data acquisition as well as data processing capabilities must be upgraded to match.

(c) Estimation of the integer ambiguity (Chapter V):

The favorable results obtained from research done in this area have dramatically reduced the associated computational burden of parallel processing the data down to a reasonably routine problem in estimation. The generalized extension of the Magill adaptive

filter, a maximum likelihood technique, was found to compare very closely with an alternative approach using an augmented state Kalman filter, except that the latter can be made optimal more conveniently through a proper initialization by accounting for all a priori information available.

B. Topic Suggestions for Future Research

While the hypothetical models used thus far have evolved with gradually-added realism throughout this development phase, there remain many facets of this project that need to be explored before it is ready for the ultimate challenge, experimental field testing. Apart from the necessary inclusion of details such as correction for atmospheric refraction and more realistic geodetic geometry, there are two major topics in particular need of attention.

The first has to do with something that was intentionally neglected in our idealized models, the effects of a less-than-perfect knowledge of the satellite-receiver geometric relations. Since the ability to resolve the integer ambiguity depends so heavily on precise information on the satellite dynamics, it is conceivable then that large uncertainties in this aspect of the filtering scheme may lead to sizable errors in the estimation of both the unknown integer and the incremental position. This source of error is concerned more with large incremental uncertainties associated with positions on the ground than errors in satellite positions which are on the whole comparatively minute.

The second topic that warrants investigation deals with the modeling

of very long baselines. So far, only models with short baselines have been handled to avoid geometric complexities. However, when the baseline considered becomes long enough, then the directional vectors at the two ends of the baseline will differ. This must be taken into account accordingly.

VII. REFERENCES

1. Vanicek, P.; and Krakiwsky, E. J. Geodesy: the Concepts. New York: North-Holland, 1982.

2. Veis, G., ed. The Use of Artificial Satellites for Geodesy. Amsterdam: North-Holland, 1963.

3. Collins, James. "Establishing First-Order Control by GPS Satellite Surveying Instruments." Technical Papers of the 43rd Annual Meeting of the American Congress on Surveying and Mapping, Washington, D.C., March 1983.

4. Remondi, Benjamin W. "GPS Geodetic Receivers - A Status Update Report." Technical Papers of the 43rd Annual Meeting of the American Congress on Surveying and Mapping, Washington, D.C., March 1983.

5. Kalman, R. E. "A New Approach to Linear Filtering and Prediction Problems." Trans. of the ASME - Journal of Basic Engr. 82, No. 1 (March 1960):35-45.

6. Brown, R. G. Introduction to Random Signal Analysis and Kalman Filtering. New York: Wiley, 1983.

7. Anderson, B. D. O.; and Moore, J. B. Optimal Filtering. Englewood Cliffs, N.J.: Prentice-Hall, 1979.

8. Gelb, A., ed. Applied Optimal Estimation. Cambridge, Mass.: MIT Press, 1974.

9. Special Issue on Applications of Kalman Filtering. IEEE Trans. on Automatic Control, AC-28, No. 3 (March 1983).

10. Magill, D. T. "Optimal Adaptive Estimation of Sampled Stochastic Processes." IEEE Trans. on Automatic Control, AC-10, No. 4 (October 1965):434-439.

11. Brown, R. G. "A New Look at the Magill Adaptive Filter as a Practical Means of Multiple Hypothesis Testing." Accepted for publication in IEEE Trans. on Circuits and Systems, CAS-30, No. 10 (October 1983).

12. Sims, F. L.; and Lainiotis, D. G. "Recursive Algorithm for the Calculation of the Adaptive Kalman Filter Weighting Coefficients." IEEE Trans. on Automatic Control, AC-14, No. 2 (April 1969):215-216.

13. Denaro, R. P.; Harvester, V. G.; Harrington, R. L. "GPS Phase I User Equipment Field Test." Journal of the Inst. of Navigation 25, No. 2 (Summer 1978):217-223.

14. Martin, E. H. "GPS User Equipment Error Models." Journal of the Inst. of Navigation 25, No. 2 (Summer 1978):201-210.

15. Special Issue on GPS. Journal of the Inst. of Navigation 25, No. 2 (Summer, 1978).

16. Denaro, R. P. "Navstar: the all-purpose satellite." IEEE Spectrum 18, No. 5 (May 1981):35-40.

17. Chrzanowski, A.; Langley, R. B.; Wells, D. E.; and McLaughlin, J. D. "A Forecast of the Impact of GPS On Surveying." Technical Papers of the 43rd Annual Meeting of the American Congress on Surveying and Mapping, Washington, D.C., March 1983.

18. Counselman, C. C.; and Gourevitch, S. A. "Miniature Interferometer Terminals for Earth Surveying: Ambiguity and Multipath with Global Positioning System." IEEE Trans. on Geoscience and Remote Sensing, GE-19, No. 4 (October 1981):244-252.

19. Rogers, A. E. E.; Knight, C. A.; Hinteregger, H. F.; Whitney, A. R.; Counselman, C. C.; Shapiro, I. I.; and Gourevitch, S. A. "Geodesy by Radio Interferometry: Determination of a 1.24-km Baseline Vector with 5-mm Repeatability." Journal of Geophysical Research 83, No. B1 (January 1978):325-334.

20. Hewlett-Packard Company. HP-87 Operating and BASIC Programming Manual (00087-90017). December 1981.

VIII. ACKNOWLEDGMENTS

The author wishes to express his profound gratitude to his major professor, Dr. R. G. Brown, for his invaluable guidance, encouraging enthusiasm, and unwavering confidence, which together contributed much to a truly fruitful research. The author is also deeply appreciative of the opportunity made possible by the financial assistance of the Electronics Affiliates Program administered by the Electrical Engineering Department of Iowa State University.

The idea of using this Kalman filtering approach to GPS geodesy as well as the formulations of the incremental GPS model originated from Dr. Brown himself. The author, in turn, was responsible for implementing the computer simulations in the early development of the model. Further, as research contribution to this thesis, the author also developed the notions of a continuous hypothesis space while addressing the problem of the computational burden posed by the original discrete solution in cases where the integer ambiguity is large. Several significant contributions from Dr. Brown are also entwined in the latter.

IX. APPENDIX A: INITIALIZING THE AUGMENTED KALMAN FILTER

From eq. 5.8, we obtain the differenced measurement model for the 3-dimensional four-satellite geometric model:

$$z_i' = D_i' \cdot x + N_i'' + v_i' \; ; \qquad i=1,2,3 \tag{9.1}$$

Recall that in the differencing scheme (eq. 4.9), z' is made up of combinations of the "raw" measurements, $z_i = \Delta\phi_i$. Now, since the latter are initially observable only as fractions of a cycle, we can assume that they each take on a uniform distribution over the interval 0 to 1. The variance of this uniform distribution is 1/12. From this, the variances of the resulting differenced measurements can be computed:

$$\begin{aligned} \mathrm{Var}(z_1') &= E[z_1'z_1'] \\ &= E[(z_1-z_2)(z_1-z_2)] \\ &= E[z_1z_1] - E[z_1z_2] - E[z_2z_1] + E[z_2z_2] \\ &= 1/12 + 0 + 0 + 1/12 \\ &= 1/6 \end{aligned}$$

$$\begin{aligned} \mathrm{Var}(z_2') &= E[z_2'z_2'] \\ &= E[(z_3-z_4)(z_3-z_4)] \\ &= E[z_3z_3] - E[z_3z_4] - E[z_4z_3] + E[z_4z_4] \\ &= 1/12 + 0 + 0 + 1/12 \\ &= 1/6 \end{aligned}$$

$$\begin{aligned}\mathrm{Var}(z_3') &= E[z_3'z_3'] \\ &= E[(z_1+z_2-z_3-z_4)(z_1+z_2-z_3-z_4)] \\ &= E[z_1z_1] + E[z_2z_2] + E[z_3z_3] + E[z_4z_4] \\ &= 1/3\end{aligned}$$

Because of the zero-mean nature of eq. 9.1, the initial state estimate vector can be set as

$$[x_1 \quad x_2 \quad x_3 \quad N_1'' \quad N_2'' \quad N_3'']^T = 0$$

As for the initial 6x6 state error covariance matrix, we consider it in 3x3 blocks. Hence,

$$\bar{P_0} = \begin{bmatrix} P_{11} & P_{12} \\ P_{21} & P_{22} \end{bmatrix}$$

The specification of P_{11} by itself constrains the values of the remaining block.

In rewriting eq. 9.1 in terms of N_i'', we ignore v_i' because its variances of 2R for i=1,2 and 4R for i=3, where $R=(1/18)^2$, were comparatively small:

$$N_i'' \cong -D_i' \cdot x + z_i' \; ; \qquad i=1,2,3$$

If we consider $P_{11} = P_x$ and $N'' \triangleq [N_1'' \quad N_2'' \quad N_3'']^T$, then

$$E[N''N''^T] = E[(-H_0x + z')(-H_0x + z')^T]$$
$$= H_0E[xx^T]H_0^T + E[z'z'^T]$$
$$= H_0P_xH_0^T + \begin{bmatrix} 1/6 & 0 & 0 \\ 0 & 1/6 & 0 \\ 0 & 0 & 1/3 \end{bmatrix}$$

$$E[x\ N''^T] = E[x\ (-H_0x + z')^T]$$
$$= -E[xx^T]H_0^T$$
$$= -\ P_xH_0^T$$

where H_0 is a matrix made up of the row vectors D_i' for i=1,2,3. Note that x and z' are taken to be uncorrelated which is true especially for large values of x.

This gives, in partitioned block form,

$$P_0^- = \begin{bmatrix} P_x & -P_xH_0^T \\ -H_0P_x^T & H_0P_xH_0^T + F \end{bmatrix} \qquad (9.2)$$

where

$$F = \begin{bmatrix} 1/6 & 0 & 0 \\ 0 & 1/6 & 0 \\ 0 & 0 & 1/3 \end{bmatrix}$$

Since this parameter reflects a condition at the initial state, the directional matrix H_0 used is that computed at t=0.

X. APPENDIX B: COMPUTER SIMULATION PROGRAMS

The simulations carried out in this project were accomplished on two computers: (1) development of the early simplified models as well as the later unknown integer estimation schemes were done on a Hewlett-Packard HP-87 personal computer which utilizes a powerful version of the BASIC computing language; (2) development of the higher-dimensional geometric models in the mid-stages of the project while still using the discrete hypotheses implementation of the Magill adaptive scheme, had to be carried out on a NAS AS-6 mainframe computer. The WATFIV version of the FORTRAN computing language was adopted in the programs run on the second machine.

The last two of the three programs selected for inclusion here contain portions developed on both computers, although, in their final form, they were reconstructed in HP-87 Basic. (The first program is also written in the same language.) Because of the similarity in the structure of BASIC to that of FORTRAN as well as the enhancements available in the HP-87 version [20], these programs can very easily be translated to FORTRAN on a virtual line-by-line basis. Additionally, only minor changes in variable names will need to be made in order to adhere to the stricter "variable type" rules in FORTRAN.

Notes for the programs:

1. The character "¢" is an exponentiation operator with the same function as "^" in standard BASIC.
2. The function RMD(x,y) gives the remainder of x/y.
3. The function INT(x) provides the largest integer $\leq$ x, e.g., INT(3.4)=3, INT(-3.4)=-4.
4. PI is a constant with the fixed value of π = 3.14159....

A. One-dimensional Single-Satellite Model with Planar Geometry

```
100 !  ##########################################################################
110 !
120 !  This program simulates the one-dimensional incremental GPS
130 !  problem using the Magill Adaptive Kalman Filter to resolve
140 !  the integer ambiguity in the carrier phase.  The formulation
150 !  of this problem may be found in the text under Section A of
160 !  Chapter IV.  The scheme here is able to pick out K.F.#4 as
170 !  the true filter that accounts for the -2 integer wavelengths
180 !  due to the incremental perturbation from the nominal.
190 !
200 !  ##########################################################################
210 !
220 !                              NOTATION
230 !         G - computer-generated Gaussian white sequence
240 !      SEED - seed of randomization
250 !       VAR - variance of the Gaussian sequence
260 !       XPR - a priori state estimate
270 !         X - updated state estimate
280 !         P - state error covariance
290 !         H - directional cosine (connection between state vector and
300 !             the measurement)
310 !         K - Kalman gain
320 !         R - variance associated with the measurement noise
330 !        PH - product of P and H
340 !        KH - product of K and H
350 !     THETA - initial elevation angle of satellite
360 !         T - time elapsed after initial measurement
370 !      TRUE - value of the true filter element (#4 in this case)
380 !       PHI - observable phase delay measurements (initially Mod 1)
390 !      PHI0 - nominal phase delay
400 !     CPROB - likelihood functions (prior conditional probabilities)
410 !      PROB - weighting coefficients (posterior conditional
420 !             probabilities)
430 !   NOMINAL - integer part of the nominal phase delay
440 !         Z - "processed" measurements (adjusted with integer
450 !             hypothesis)
460 !       RES - measurement residual
470 ! VARIANCE - variance of the measurement residual
480 !     TOTAL - summation of CPROB for normalization in getting PROB
490 !         I - observation time steps
500 !         F - filter element counter
510 !
520 !
530 !           GENERATING THE RANDOM SEQUENCE
540 !
550 DIM G(110),PHI(55),CPROB(11),PROB(11),XPR(11),X(11)
560 SEED=13
```

```
570 BIG=10000000000
580 RAD
590 VAR=(1/18)¢2
600 FOR I=0 TO 55
610    S=SEED
620    SEED=RMD (51*S+7,BIG)
630    SCL1=SEED/BIG
640    S=SEED
650    SEED=RMD (51*S+7,BIG)
660    SCL2=SEED/BIG
670    IF I<6 THEN 710
680    RN=SQR (2*VAR*LOG (1/SCL1))
690    G(I*2-12)=RN*COS (2*PI *SCL2)
700    G(I*2-11)=RN*SIN (2*PI *SCL2)
710 NEXT I
720 !
730 !
740 !          SIMULATING THE PHASE MEASUREMENTS
750 !
760 DEG
770 THETA=30 @ TRUE=4
780 FOR I=0 TO 50
790    T=20*I
800    PHI(I)=102.5*COS (THETA+T/120)-IP (102.5*COS (THETA))+G(I)
810 NEXT I
820 !
830 !
840 !        INITIALIZING THE FILTER
850 !
860 PPR=4 @ R=VAR
870 FOR F=1 TO 11
880    CPROB(F)=1 @ XPR(F)=0
890 NEXT F
900 NOMINAL=IP (100*COS (THETA))
910 !
920 !
930 !        THE KALMAN FILTER DOMAIN (COMMON COVARIANCE
940 !                    AND GAIN STRUCTURE)
950 !
960 FOR I=0 TO 50
970    T=20*I
980    PHI0=100*COS (THETA+T/120)-NOMINAL
990    H=COS (THETA+T/120)
1000    VARIANCE=H¢2*PPR+R
1010    K=PPR*H/VARIANCE
1020    P=(1-K*H)*PPR
1030    TOTAL=0
1040 !
1050 !
1060 !     THE DISCRETE HYPOTHESIS LOOP (THE MAGILL ADAPTIVE SCHEME)
```

```
1070 !
1080    FOR F=1 TO 11
1090       Z=PHI(I)-(PHI0+(F-6))
1100       RES=Z-H*XPR(F)
1110       XPR(F)=XPR(F)+K*RES
1120       CPROB(F)=CPROB(F)*EXP (-(RES¢2/2/VARIANCE))
1130       TOTAL=TOTAL+CPROB(F)
1140    NEXT F
1150    FOR F=1 TO 11
1160 !
1170 !
1180 !        CALCULATING THE WEIGHTING COEFFICIENTS
1190 !
1200       PROB(F)=CPROB(F)/TOTAL
1210    NEXT F
1220    PPR=P
1230    PRINT PROB(TRUE)
1240 NEXT I
1250 END
```

B. Three-dimensional Four-Satellite Model
(Preliminary Estimation with Maximum Likelihood Method)

```
1000 ! ##########################################################################
1010 !
1020 ! This program simulates the 3-dimensional geometric model formu-
1030 ! lated in the text under Section B of Chapter IV.  The processing
1040 ! scheme first undergoes a preliminary run to estimate the unknown
1050 ! integer vector using the maximum likelihood method derived in
1060 ! Chapter V (section A).  The notation described below draws
1070 ! heavily from the given references.
1080 !
1090 ! The program begins with the simulation of the phase measurements
1100 ! with computer-generated random numbers.  The first part of the
1110 ! processing portion, as mentioned above, estimates the unknown
1120 ! integer vector, while the second, utilizing this estimate, runs
1130 ! the discrete hypotheses in a parallel structure similar to that
1140 ! in the program listed in Appendix C.
1150 !
1160 ! ##########################################################################
1170 !
```

```
1180 !
1190 !                                NOTATION
1200 !
1210 !         G - computer-generated Gaussian white sequence
1220 !      SEED - seed of randomization
1230 !       VAR - variance of the Gaussian sequence
1240 !   PHI1234 - raw phase measurements
1250 !      DPHI - differenced phase measurements
1260 !      PHI0 - nominal phase delay
1270 !        ZM - measured phase less the nominal phase
1280 !             (differenced version)
1290 !       PPR - a priori state error covariance matrix
1300 !         P - updated state error covariance matrix
1310 !      GAIN - Kalman gain
1320 !         H - linear connection matrix between the state and the
1330 !             differenced measurements (made up of differenced
1340 !             directional vectors)
1350 !       PKH - matrix product of GAIN and H
1360 !        PH - matrix product of PPR and transposed H
1370 ! CX,CY,CZ - directional cosine vectors in 3-dimensional space
1380 !        CF - 4x4 coefficient matrix of the state vector
1390 !             ( C b  in text)
1400 !      LKHD - quadratic weighting matrix formed from the log-
1410 !             likelihood function (W(k) in text)
1420 !         V - covariance associated with the measurement residual
1430 !  FIX1234 - integer values of the nominal phase delay
1440 ! QFIX1234 - integer values of the actual phase delay
1450 !       PI2 - twice the value of PI
1460 !        R2 - twice the variance of the raw measurement noise
1470 !      ANLY - upper-left 3x3 block of the 4x4 LKHD matrix
1480 !      AINV - inverse matrix of ANLY
1490 !        PT - final estimate of the unknown integer vector
1500 !      TEMP - used as intermediate variable in several calculations
1510 !        MX - maximum number of processing steps
1520 ! DX,DY,DZ - incremental perturbation from nominal baseline in
1530 !             3-dimensional space
1540 !        DT - time elapsed after initial measurement
1550 !     CLOCK - clock bias
1560 !        FX - coordinate indices of the eight "integer locations"
1570 !             making up a unit cube
1580 !     XLKHD - actual log-likelihood values computed at FX locations
1590 !        NR - true integer location resulting from comparison of
1600 !             XLKHD at the locations in FX
1610 !       XPR - state estimate vector of the true element NR (this is
1620 !             the desired result)
1630 !
1640 !
1650 !
1660 DIM DPHI(3,51),PPR(3,3),PHI0(4),PKH(3,3),GAIN(3,3),ZM(3),TEMP(4)
1670 DIM XPR(3),FX(3,10),XLKHD(10),HX(4),CF(4,4),LKHD(4,4),V(3),PT(3)
```

```
1680 DIM P(3,3),H(3,3),G(205),PH(3),CX(4),CY(4),CZ(4),ANLY(3,4)
1690 DIM AINV(3,3)
1700 !
1710 !
1720 !              GENERATING THE RANDOM SEQUENCE
1730 !
1740 SEED=13 @ MX=51 @ BIG=10000000000
1750 RAD
1760 VAR=(1/18)↑2
1770 FOR I=1 TO MX*2+5
1780    S=SEED
1790    SEED=RMD (51*S+7,BIG)
1800    SCL1=SEED/BIG
1810    S=SEED
1820    SEED=RMD (51*S+7,BIG)
1830    SCL2=SEED/BIG
1840    IF I<6 THEN 1880
1850    RN=SQR (2*VAR*LOG (1/SCL1))
1860    G(2*I-11)=RN*COS (2*PI *SCL2)
1870    G(2*I-10)=RN*SIN (2*PI *SCL2)
1880 NEXT I
1890 PI2=2*PI
1900 !
1910 !
1920 !                    INITIAL SATELLITE ANGLES
1930 !
1940 DEG
1950 ALFA1=15 @ ALFA2=75 @ BETA1=90 @ BETA2=150
1960 THET1=0 @ THET2=60 @ CLOCK=.25
1970 !
1980 !
1990 !    SIMULATING THE PHASE MEASUREMENTS  The baseline vector
2000 !      is (100,0,0) and the perturbation vector is (1.5,1.5,1.5)
2010 !
2020 DX=1.5 @ DY=1.5 @ DZ=1.5
2030 DT=0
2040 GOSUB DRNCOS
2050 FIX1=(100+DX)*CX(1)+DY*CY(1)+DZ*CZ(1)+CLOCK
2060 FIX2=(100+DX)*CX(2)+DY*CY(2)+DZ*CZ(2)+CLOCK
2070 FIX3=(100+DX)*CX(3)+DY*CY(3)+DZ*CZ(3)+CLOCK
2080 FIX4=(100+DX)*CX(4)+DY*CY(4)+DZ*CZ(4)+CLOCK
2090 FIX1=INT (FIX1) @ FIX2=INT (FIX2)
2100 FIX3=INT (FIX3) @ FIX4=INT (FIX4)
2110 FOR I=1 TO MX
2120    DT=(I-1)/6
2130    GOSUB DRNCOS
2140    PHI1=(100+DX)*CX(1)+DY*CY(1)+DZ*CZ(1)+CLOCK-FIX1+G(4*I-3)
2150    PHI2=(100+DX)*CX(2)+DY*CY(2)+DZ*CZ(2)+CLOCK-FIX2+G(4*I-2)
2160    PHI3=(100+DX)*CX(3)+DY*CY(3)+DZ*CZ(3)+CLOCK-FIX3+G(4*I-1)
2170    PHI4=(100+DX)*CX(4)+DY*CY(4)+DZ*CZ(4)+CLOCK-FIX4+G(4*I)
```

```
2180    DPHI(1,I)=PHI1-PHI2 @ DPHI(2,I)=PHI3-PHI4
2190    DPHI(3,I)=PHI1+PHI2-PHI3-PHI4
2200 NEXT I
2210 !
2220 !
2230 !              INITIALIZING THE FILTER
2240 !
2250 FOR I=1 TO 3
2260    FOR J=1 TO 3
2270       IF I=J THEN PPR(I,J)=4 ELSE PPR(I,J)=0
2280    NEXT J
2290 NEXT I
2300 FOR N=1 TO 4
2310    FOR NN=1 TO 4
2320       CF(N,NN)=0 @ LKHD(N,NN)=0
2330    NEXT NN
2340 NEXT N
2350 R2=2*(1/18)↑2
2360 DT=0
2370 GOSUB DRNCOS
2380 QFIX1=100*CX(1) @ QFIX2=100*CX(2)
2390 QFIX3=100*CX(3) @ QFIX4=100*CX(4)
2400 QFIX1=INT (QFIX1) @ QFIX2=INT (QFIX2)
2410 QFIX3=INT (QFIX3) @ QFIX4=INT (QFIX4)
2420 !
2430 !
2440 !         THE PROCESSING LOOP
2450 !
2460 FOR I=1 TO MX
2470    DT=(I-1)/6
2480    GOSUB DRNCOS
2490    H(1,1)=CX(1)-CX(2)
2500    H(1,2)=CY(1)-CY(2)
2510    H(1,3)=CZ(1)-CZ(2)
2520    H(2,1)=CX(3)-CX(4)
2530    H(2,2)=CY(3)-CY(4)
2540    H(2,3)=CZ(3)-CZ(4)
2550    H(3,1)=CX(1)+CX(2)-CX(3)-CX(4)
2560    H(3,2)=CY(1)+CY(2)-CY(3)-CY(4)
2570    H(3,3)=CZ(1)+CZ(2)-CZ(3)-CZ(4)
2580    PHI0(1)=100*CX(1)-QFIX1 @ PHI0(2)=100*CX(2)-QFIX2
2590    PHI0(3)=100*CX(3)-QFIX3 @ PHI0(4)=100*CX(4)-QFIX4
2600 !
2610 !
2620 !       THE SEQUENTIAL PROCESSING LOOP
2630 !
2640    FOR M=1 TO 3
2650       FOR N=1 TO 3
2660          PH(N)=PPR(N,1)*H(M,1)+PPR(N,2)*H(M,2)+PPR(N,3)*H(M,3)
2670       NEXT N
```

```
2680        V(M)=H(M,1)*PH(1)+H(M,2)*PH(2)+H(M,3)*PH(3)+R2
2690        IF M=3 THEN V(M)=V(M)+R2
2700        GAIN(1,M)=PH(1)/V(M) @ GAIN(2,M)=PH(2)/V(M)
2710        GAIN(3,M)=PH(3)/V(M)
2720        IF M=1 THEN ZM(1)=DPHI(M,I)-(PHIO(1)-PHIO(2))
2730        IF M=2 THEN ZM(2)=DPHI(M,I)-(PHIO(3)-PHIO(4))
2740        IF M=3 THEN ZM(3)=DPHI(M,I)-(PHIO(1)+PHIO(2)-PHIO(3)-PHIO(4))
2750        FOR N=1 TO 4
2760           HX(N)=-(H(M,1)*CF(1,N)+H(M,2)*CF(2,N)+H(M,3)*CF(3,N))
2770           IF M=N THEN HX(N)=HX(N)-1
2780           IF N=4 THEN HX(4)=HX(4)+ZM(M)
2790 !
2800 !
2810 ! UPDATING THE COEFFICIENT MATRIX
2820 !
2830           FOR NN=1 TO 3
2840              CF(NN,N)=CF(NN,N)+GAIN(NN,M)*HX(N)
2850           NEXT NN
2860        NEXT N
2870 !
2880 !
2890 ! UPDATING THE (LOG-LIKELIHOOD) QUADRATIC WEIGHTING MATRIX
2900 !
2910        FOR N=1 TO 4
2920           FOR NN=1 TO 4
2930              LKHD(N,NN)=LKHD(N,NN)+HX(N)*HX(NN)/2/V(M)
2940           NEXT NN
2950        NEXT N
2960 !
2970 !
2980 ! UPDATING THE (KALMAN FILTER) STATE ERROR COVARIANCE MATRIX
2990 !
3000        FOR N=1 TO 3
3010           FOR NN=1 TO 3
3020              PKH(N,NN)=-(GAIN(N,M)*H(M,NN))
3030              IF N=NN THEN PKH(N,NN)=1+PKH(N,NN)
3040           NEXT NN
3050        NEXT N
3060        FOR N=1 TO 3
3070           FOR NN=1 TO 3
3080              TTEMP=PKH(N,1)*PPR(1,NN)+PKH(N,2)*PPR(2,NN)
3090              P(N,NN)=TTEMP+PKH(N,3)*PPR(3,NN)
3100           NEXT NN
3110        NEXT N
3120        FOR N=1 TO 3
3130           FOR NN=1 TO 3
3140              PPR(N,NN)=P(N,NN)
3150           NEXT NN
3160        NEXT N
3170     NEXT M
```

```
3180 NEXT I
3190 !
3200 !   END OF PROCESSING LOOP
3210 !
3220 ! ***************************************************************************************
3230 !
3240 !   ESTIMATE THE UNKNOWN INTEGER VECTOR FROM
3250 !     THE FINAL QUADRATIC WEIGHTING MATRIX
3260 !
3270 FOR M=1 TO 3
3280    FOR N=1 TO 4
3290       ANLY(M,N)=2*LKHD(M,N)
3300    NEXT N
3310 NEXT M
3320 GOSUB INVERSE
3330 FOR M=1 TO 3
3340    TTEMP=-(AINV(M,1)*ANLY(1,4))-AINV(M,2)*ANLY(2,4)
3350    PT(M)=TTEMP-AINV(M,3)*ANLY(3,4)
3360 NEXT M
3370 !
3380 !
3390 !      SETTING UP THE HYPOTHESES (EIGHT "INTEGER" LOCATIONS)
3400 !              FOR THE MAGILL ADAPTIVE FILTER SCHEME
3410 !
3420 IX1=INT (PT(1)) @ IX2=INT (PT(2)) @ IX3=INT (PT(3))
3430 FX(1,1)=IX1 @ FX(2,1)=IX2 @ FX(3,1)=IX3
3440 FX(1,2)=IX1+1 @ FX(2,2)=IX2 @ FX(3,2)=IX3
3450 FX(1,3)=IX1 @ FX(2,3)=IX2+1 @ FX(3,3)=IX3
3460 FX(1,4)=IX1+1 @ FX(2,4)=IX2+1 @ FX(3,4)=IX3
3470 FX(1,5)=IX1 @ FX(2,5)=IX2 @ FX(3,5)=IX3+1
3480 FX(1,6)=IX1+1 @ FX(2,6)=IX2 @ FX(3,6)=IX3+1
3490 FX(1,7)=IX1 @ FX(2,7)=IX2+1 @ FX(3,7)=IX3+1
3500 FX(1,8)=IX1+1 @ FX(2,8)=IX2+1 @ FX(3,8)=IX3+1
3510 !
3520 !
3530 !    ALL THE NECESSARY PARAMETER VALUES FOR THE MAGILL ADAPTIVE
3540 !    SCHEME CAN BE OBTAINED FROM THE FUNCTIONS LKHD AND CF
3550 !    ALREADY COMPUTED ABOVE IN THE MAXIMUM LIKELIHOOD ESTIMATOR
3560 !
3570 FOR L=1 TO 8
3580    FOR M=1 TO 4
3590       TTEMP=LKHD(M,1)*FX(1,L)+LKHD(M,2)*FX(2,L)
3600       TEMP(M)=TTEMP+LKHD(M,3)*FX(3,L)+LKHD(M,4)
3610    NEXT M
3620    XLKHD(L)=FX(1,L)*TEMP(1)+FX(2,L)*TEMP(2)+FX(3,L)*TEMP(3)+TEMP(4)
3630 NEXT L
3640 !
3650 !
3660 !           COMPARING XLKHD AMONG THE EIGHT FX LOCATIONS
3670 !
```

```
3680 NR=1 @ XMIN=XLKHD(1)
3690 FOR L=2 TO 8
3700    IF XLKHD(L)>= XMIN THEN 3720
3710    XMIN=XLKHD(L) @ NR=L
3720 NEXT L
3730 FOR M=1 TO 3
3740   XPR(M)=CF(M,1)*FX(1,NR)+CF(M,2)*FX(2,NR)+CF(M,3)*FX(3,NR)+CF(M,4)
3750 NEXT M
3760 PRINT XPR(1),XPR(2),XPR(3)
3770 END
3780 !
3790 !
3800 !
3810 !
3820 !     THE SUBROUTINE "INVERSE" INVERTS A 3x3 MATRIX
3830 !
3840 INVERSE:
3850    DET1=ANLY(1,1)*(ANLY(2,2)*ANLY(3,3)-ANLY(2,3)*ANLY(3,2))
3860    DET2=ANLY(1,2)*(ANLY(2,1)*ANLY(3,3)-ANLY(2,3)*ANLY(3,1))
3870    DET3=ANLY(1,3)*(ANLY(2,1)*ANLY(3,2)-ANLY(2,2)*ANLY(3,1))
3880    DET=DET1-DET2+DET3
3890    AINV(1,1)=(ANLY(2,2)*ANLY(3,3)-ANLY(2,3)*ANLY(3,2))/DET
3900    AINV(2,2)=(ANLY(1,1)*ANLY(3,3)-ANLY(1,3)*ANLY(3,1))/DET
3910    AINV(3,3)=(ANLY(1,1)*ANLY(2,2)-ANLY(1,2)*ANLY(2,1))/DET
3920    AINV(1,2)=-((ANLY(1,2)*ANLY(3,3)-ANLY(1,3)*ANLY(3,2))/DET)
3930    AINV(1,3)=(ANLY(1,2)*ANLY(2,3)-ANLY(1,3)*ANLY(2,2))/DET
3940    AINV(2,1)=-((ANLY(2,1)*ANLY(3,3)-ANLY(2,3)*ANLY(3,1))/DET)
3950    AINV(2,3)=-((ANLY(1,1)*ANLY(2,3)-ANLY(1,3)*ANLY(2,1))/DET)
3960    AINV(3,1)=(ANLY(2,1)*ANLY(3,2)-ANLY(2,2)*ANLY(3,1))/DET
3970    AINV(3,2)=-((ANLY(1,1)*ANLY(3,2)-ANLY(1,2)*ANLY(3,1))/DET)
3980 RETURN
3990 !
4000 !
4010 !  THE SUBROUTINE "DRNCOS" COMPUTES THE DIRECTION COSINE VECTORS
4020 !  OF THE SATELLITES BASED ON THE SPECIFIED INITIAL ANGLES AND
4030 !  GIVEN THE ELAPSED TIME, DT.
4040 !
4050 DRNCOS:
4060    CA1=COS (ALFA1+DT) @ CA2=COS (ALFA2+DT)
4070    SA1=SIN (ALFA1+DT) @ SA2=SIN (ALFA2+DT)
4080    CB1=COS (BETA1+DT) @ CB2=COS (BETA2+DT)
4090    SB1=SIN (BETA1+DT) @ SB2=SIN (BETA2+DT)
4100    CT1=COS (THET1+DT/2) @ CT2=COS (THET2-DT/2)
4110    ST1=SIN (THET1+DT/2) @ ST2=SIN (THET2-DT/2)
4120    CX(1)=CA1*CT1+SA1*ST1/2 @ CY(1)=-(CA1*ST1)+SA1*CT1/2
4130    CZ(1)=.866*SA1
4140    CX(2)=CA2*CT1+SA2*ST1/2 @ CY(2)=-(CA2*ST1)+SA2*CT1/2
4150    CZ(2)=.866*SA2
4160    CX(3)=-(CB1*CT2)+SB1*ST2/2 @ CY(3)=-(CB1*ST2)-SB1*CT2/2
4170    CZ(3)=.866*SB1
```

```
4180     CX(4)=-(CB2*CT2)+SB2*ST2/2 @ CY(4)=-(CB2*ST2)-SB2*CT2/2
4190     CZ(4)=.866*SB2
4200 RETURN
```

C. Three-dimensional Four-Satellite Model (Preliminary Estimation with Augmented Kalman Filter)

```
1000 ! ##########################################################################
1010 !
1020 ! This program consists of the simulation of phase measurements
1030 ! based on the 3-dimensional geometric model of Chapter IV (section
1040 ! B), and the six-state augmented Kalman filter described in
1050 ! Chapter V (section B).
1060 !
1070 ! The program begins by simulating the measurements with the aid of
1080 ! computer-generated random numbers.  The next part of the program
1090 ! makes up the six-state Kalman filter used to process the simu-
1100 ! lated measurements with the preliminary objective of estimating
1110 ! only the unknown integer vector (the augmented portion of the
1120 ! state).  The discrete Magill adaptive scheme, with eight filters
1130 ! geometrically placed at the corners of a unit cube "surrounding"
1140 ! the final estimate computed of the unknown integer vector, rounds
1150 ! up the last part of the program with the intention of estimating
1160 ! the 3-tuple state vector representing the incremental position
1170 ! perturbation.
1180 !
1190 ! ##########################################################################
1200 !
1210 !
1220 !                          NOTATION
1230 !
1240 !         G - computer-generated Gaussian white sequence
1250 !      SEED - seed of randomization
1260 !       VAR - variance of the Gaussian sequence
1270 !   PHI1234 - raw phase measurements
1280 !      DPHI - differenced phase measurements
1290 !      PHI0 - nominal phase delay
1300 !        ZM - measured phase less the nominal phase
1310 !             (differenced version)
1320 !       RES - measurement residual
1330 !         V - error covariance associated with the measurement
1340 !             residual
```

```
1350 !       PPR - a priori state error covariance matrix
1360 !         P - updated state error covariance matrix
1370 !      GAIN - Kalman gain
1380 !         H - linear connection matrix between the state and the
1390 !             differenced measurements (made up of differenced
1400 !             directional vectors)
1410 !       PKH - matrix product of GAIN and H
1420 !        PH - matrix product of PPR and transposed H
1430 ! CX,CY,CZ - directional cosine vectors in 3-dimensional space
1440 !  FIX1234 - integer values of the nominal phase delay
1450 ! QFIX1234 - integer values of the actual phase delay
1460 !  IFIX123 - true value of the unknown integer vector(used for
1470 !             checking against the solution obtained)
1480 !       PI2 - twice the value of PI
1490 !        R2 - twice the variance of the raw phase measurement noise
1500 !        MX - total number of processing steps
1510 ! DX,DY,DZ - incremental position perturbation from nominal baseline
1520 !             in 3-dimensional space
1530 !        DT - time elapsed after initial measurement
1540 !     CLOCK - clock bias (error)
1550 !      AXPR - 6-tuple state vector (3-position augmented with
1560 !             3-tuple hypothesis vector)
1570 !       XPR - 3-tuple state vector used in the Magill adaptive scheme
1580 !             in the final part of the program
1590 !        FX - coordinate indices of the eight "integer locations"
1600 !             making up a unit cube
1610 !     XLKHD - actual log-likelihood values computed at FX locations
1620 !        NR - true integer location resulting from comparison of
1630 !             XLKHD at the locations in FX
1640 !
1650 !
1660 !
1670 !
1680 DIM DPHI(3,51),PPR(6,6),PHI0(4),PKH(6,6),GAIN(6),ZM(3,51),AXPR(6)
1690 DIM P(6,6),H(3,6),G(205),PH(6),CX(4),CY(4),CZ(4),XPR(8,3),PC(3,3)
1700 DIM FX(8,3),XLKHD(8)
1710 !
1720 !
1730 !         GENERATING THE RANDOM SEQUENCE
1740 !
1750 SEED=13 @ MX=51 @ BIG=10000000000
1760 RAD
1770 VAR=(1/18)¢2
1780 FOR I=1 TO MX*2+5
1790    S=SEED
1800    SEED=RMD (51*S+7,BIG)
1810    SCL1=SEED/BIG
1820    S=SEED
1830    SEED=RMD (51*S+7,BIG)
1840    SCL2=SEED/BIG
```

```
1850    IF I<6 THEN 1890
1860    RN=SQR (2*VAR*LOG (1/SCL1))
1870    G(2*I-11)=RN*COS (2*PI *SCL2)
1880    G(2*I-10)=RN*SIN (2*PI *SCL2)
1890 NEXT I
1900 PI2=2*PI
1910 !
1920 !
1930 !         INITIAL SATELLITE ANGLES
1940 !
1950 DEG
1960 ALFA1=15 @ ALFA2=75 @ BETA1=90 @ BETA2=150
1970 THET1=0 @ THET2=60 @ CLOCK=.25
1980 !
1990 !
2000 !         SIMULATING THE PHASE MEASUREMENTS
2010 !         The nominal baseline vector is (100,0,0) with
2020 !         an incremental position perturbation of (1.5,1.5,1.5)
2030 !
2040 DX=1.5 @ DY=1.5 @ DZ=1.5
2050 DT=0
2060 GOSUB DRNCOS
2070 FIX1=(100+DX)*CX(1)+DY*CY(1)+DZ*CZ(1)+CLOCK
2080 FIX2=(100+DX)*CX(2)+DY*CY(2)+DZ*CZ(2)+CLOCK
2090 FIX3=(100+DX)*CX(3)+DY*CY(3)+DZ*CZ(3)+CLOCK
2100 FIX4=(100+DX)*CX(4)+DY*CY(4)+DZ*CZ(4)+CLOCK
2110 FIX1=INT (FIX1) @ FIX2=INT (FIX2) @ FIX3=INT (FIX3) @ FIX4=INT (FIX4)
2120 FOR I=1 TO MX
2130    DT=(I-1)/6
2140    GOSUB DRNCOS
2150    PHI1=(100+DX)*CX(1)+DY*CY(1)+DZ*CZ(1)+CLOCK-FIX1+G(4*I-3)
2160    PHI2=(100+DX)*CX(2)+DY*CY(2)+DZ*CZ(2)+CLOCK-FIX2+G(4*I-2)
2170    PHI3=(100+DX)*CX(3)+DY*CY(3)+DZ*CZ(3)+CLOCK-FIX3+G(4*I-1)
2180    PHI4=(100+DX)*CX(4)+DY*CY(4)+DZ*CZ(4)+CLOCK-FIX4+G(4*I)
2190    DPHI(1,I)=PHI1-PHI2 @ DPHI(2,I)=PHI3-PHI4
2200    DPHI(3,I)=PHI1+PHI2-PHI3-PHI4
2210 NEXT I
2220 !
2230 !           THE AUGMENTED KALMAN FILTER:
2240 !    INITIALIZING THE STATE ERROR COVARIANCE MATRIX
2250 !           Details are given in Appendix B
2260 !
2270 DT=0
2280 GOSUB DRNCOS
2290 H(1,1)=CX(1)-CX(2)
2300 H(1,2)=CY(1)-CY(2)
2310 H(1,3)=CZ(1)-CZ(2)
2320 H(2,1)=CX(3)-CX(4)
2330 H(2,2)=CY(3)-CY(4)
2340 H(2,3)=CZ(3)-CZ(4)
```

```
2350 H(3,1)=CX(1)+CX(2)-CX(3)-CX(4)
2360 H(3,2)=CY(1)+CY(2)-CY(3)-CY(4)
2370 H(3,3)=CZ(1)+CZ(2)-CZ(3)-CZ(4)
2380 FOR I=1 TO 3
2390    FOR J=1 TO 3
2400       IF I=J THEN PPR(I,J)=4 ELSE PPR(I,J)=0
2410    NEXT J
2420 NEXT I
2430 FOR I=1 TO 3
2440    FOR J=1 TO 3
2450       PPR(I,J+3)=-(PPR(I,1)*H(J,1)+PPR(I,2)*H(J,2)+PPR(I,3)*H(J,3))
2460       PPR(J+3,I)=PPR(I,J+3)
2470    NEXT J
2480 NEXT I
2490 FOR I=1 TO 3
2500    FOR J=1 TO 3
2510       PC(I,J)=PPR(I,1)*H(J,1)+PPR(I,2)*H(J,2)+PPR(I,3)*H(J,3)
2520    NEXT J
2530 NEXT I
2540 FOR I=1 TO 3
2550    FOR J=1 TO 3
2560       PPR(I+3,J+3)=H(I,1)*PC(1,J)+H(I,2)*PC(2,J)+H(I,3)*PC(3,J)
2570       IF I=J THEN PPR(I+3,J+3)=PPR(I+3,J+3)+1/12
2580    NEXT J
2590 NEXT I
2600 !
2610 !
2620 !     INITIALIZING THE STATE VECTOR
2630 !
2640 R2=2*(1/18)↑2
2650 FOR I=1 TO 6
2660    AXPR(I)=0
2670 NEXT I
2680 DT=0
2690 GOSUB DRNCOS
2700 QFIX1=100*CX(1) @ QFIX2=100*CX(2)
2710 QFIX3=100*CX(3) @ QFIX4=100*CX(4)
2720 QFIX1=INT (QFIX1) @ QFIX2=INT (QFIX2)
2730 QFIX3=INT (QFIX3) @ QFIX4=INT (QFIX4)
2740 !
2750 !
2760 !     COMPUTING THE TRUE VALUE OF THE UNKNOWN INTEGER
2770 !      FOR PURPOSES OF CHECKING AGAINST THE SOLUTION
2780 !
2790 IFIX1=QFIX1-FIX1-(QFIX2-FIX2)
2800 IFIX2=QFIX3-FIX3-(QFIX4-FIX4)
2810 IFIX3=QFIX1-FIX1+(QFIX2-FIX2)-(QFIX3-FIX3+(QFIX4-FIX4))
2820 PRINT IFIX1,IFIX2,IFIX3
2830 !
2840 !
```

```
2850 !     SETTING UP THE AUGMENTED PORTION OF THE H-MATRIX
2860 !
2870 FOR I=1 TO 3
2880    FOR J=4 TO 6
2890       IF I=J-3 THEN H(I,J)=1 ELSE H(I,J)=0
2900    NEXT J
2910 NEXT I
2920 !
2930 !
2940 !     THE PROCESSING LOOP
2950 !
2960 FOR I=1 TO MX
2970    DT=(I-1)/6
2980    GOSUB DRNCOS
2990    H(1,1)=CX(1)-CX(2)
3000    H(1,2)=CY(1)-CY(2)
3010    H(1,3)=CZ(1)-CZ(2)
3020    H(2,1)=CX(3)-CX(4)
3030    H(2,2)=CY(3)-CY(4)
3040    H(2,3)=CZ(3)-CZ(4)
3050    H(3,1)=CX(1)+CX(2)-CX(3)-CX(4)
3060    H(3,2)=CY(1)+CY(2)-CY(3)-CY(4)
3070    H(3,3)=CZ(1)+CZ(2)-CZ(3)-CZ(4)
3080    PHI0(1)=100*CX(1)-QFIX1 @ PHI0(2)=100*CX(2)-QFIX2
3090    PHI0(3)=100*CX(3)-QFIX3 @ PHI0(4)=100*CX(4)-QFIX4
3100 !
3110 !
3120 !     THE SEQUENTIAL PROCESSING LOOP
3130 !
3140    FOR M=1 TO 3
3150 !
3160 !
3170 ! COMPUTING THE KALMAN GAIN
3180 !
3190       FOR N=1 TO 6
3200          TOTAL=0
3210          FOR NN=1 TO 6
3220             TOTAL=TOTAL+PPR(N,NN)*H(M,NN)
3230          NEXT NN
3240          PH(N)=TOTAL
3250       NEXT N
3260       TOTAL=0
3270       FOR N=1 TO 6
3280          TOTAL=TOTAL+H(M,N)*PH(N)
3290       NEXT N
3300       V(M)=TOTAL+R2
3310       IF M=3 THEN V(M)=V(M)+R2
3320       FOR N=1 TO 6
3330          GAIN(N)=PH(N)/V(M)
3340       NEXT N
```

```
3350 !
3360 !
3370 ! THE STATE ESTIMATE UPDATE
3380 !
3390       IF M=1 THEN ZM(1,I)=DPHI(M,I)-(PHIO(1)-PHIO(2))
3400       IF M=2 THEN ZM(2,I)=DPHI(M,I)-(PHIO(3)-PHIO(4))
3410       IF M=3 THEN ZM(3,I)=DPHI(M,I)-(PHIO(1)+PHIO(2)-PHIO(3)-PHIO(4))
3420       TOTAL=0
3430       FOR N=1 TO 6
3440          TOTAL=TOTAL+H(M,N)*AXPR(N)
3450       NEXT N
3460       RES=ZM(M,I)-TOTAL
3470       FOR N=1 TO 6
3480          AXPR(N)=AXPR(N)+GAIN(N)*RES
3490       NEXT N
3500 !
3510 !
3520 ! THE STATE ERROR COVARIANCE UPDATE
3530 !
3540       FOR N=1 TO 6
3550          FOR NN=1 TO 6
3560             PKH(N,NN)=-(GAIN(N)*H(M,NN))
3570             IF N=NN THEN PKH(N,NN)=1+PKH(N,NN)
3580          NEXT NN
3590       NEXT N
3600       FOR N=1 TO 6
3610          FOR NN=1 TO 6
3620             TOTAL=0
3630             FOR NNN=1 TO 6
3640                TOTAL=TOTAL+PKH(N,NNN)*PPR(NNN,NN)
3650             NEXT NNN
3660             P(N,NN)=TOTAL
3670          NEXT NN
3680       NEXT N
3690       FOR N=1 TO 6
3700          FOR NN=1 TO 6
3710             PPR(N,NN)=P(N,NN)
3720          NEXT NN
3730       NEXT N
3740    NEXT M
3750 NEXT I
3760 !
3770 !
3780 ! END OF PROCESSING LOOP
3790 !
3800 ! OUTPUT: THE FINAL ESTIMATE OF THE UNKNOWN INTEGER VECTOR
3810 !
3820 PRINT AXPR(4),AXPR(5),AXPR(6)
3830 !
3840 !
```

```
3850 ! ***************************************************************************
3860 !              THE MAGILL ADAPTIVE SCHEME
3870 !
3880 !       SETTING UP THE EIGHT "INTEGER LOCATIONS" AT THE CORNERS
3890 !       OF A UNIT CUBE GEOMETRICALLY CONTAINING THE FINAL ESTIMATE
3900 !       FOUND ABOVE
3910 !
3920 IX1=INT (AXPR(4)) @ IX2=INT (AXPR(5)) @ IX3=INT (AXPR(6))
3930 FX(1,1)=IX1 @ FX(1,2)=IX2 @ FX(1,3)=IX3
3940 FX(2,1)=IX1+1 @ FX(2,2)=IX2 @ FX(2,3)=IX3
3950 FX(3,1)=IX1 @ FX(3,2)=IX2+1 @ FX(3,3)=IX3
3960 FX(4,1)=IX1+1 @ FX(4,2)=IX2+1 @ FX(4,3)=IX3
3970 FX(5,1)=IX1 @ FX(5,2)=IX2 @ FX(5,3)=IX3+1
3980 FX(6,1)=IX1+1 @ FX(6,2)=IX2 @ FX(6,3)=IX3+1
3990 FX(7,1)=IX1 @ FX(7,2)=IX2+1 @ FX(7,3)=IX3+1
4000 FX(8,1)=IX1+1 @ FX(8,2)=IX2+1 @ FX(8,3)=IX3+1
4010 !
4020 !
4030 !   INITIALIZATION OF THE FILTER
4040 !
4050 FOR I=1 TO 3
4060    FOR J=1 TO 3
4070       IF I=J THEN PPR(I,J)=4 ELSE PPR(I,J)=0
4080    NEXT J
4090 NEXT I
4100 FOR I=1 TO 8
4110    XPR(I,1),XPR(I,2),XPR(I,3)=0
4120    XLKHD(I)=0
4130 NEXT I
4140 !
4150 !
4160 !   THE PROCESSING LOOP
4170 !
4180 FOR I=1 TO MX
4190    DT=(I-1)/6
4200    GOSUB DRNCOS
4210    H(1,1)=CX(1)-CX(2)
4220    H(1,2)=CY(1)-CY(2)
4230    H(1,3)=CZ(1)-CZ(2)
4240    H(2,1)=CX(3)-CX(4)
4250    H(2,2)=CY(3)-CY(4)
4260    H(2,3)=CZ(3)-CZ(4)
4270    H(3,1)=CX(1)+CX(2)-CX(3)-CX(4)
4280    H(3,2)=CY(1)+CY(2)-CY(3)-CY(4)
4290    H(3,3)=CZ(1)+CZ(2)-CZ(3)-CZ(4)
4300 !
4310 !
4320 ! THE SEQUENTIAL PROCESSING LOOP
4330 !
4340    FOR M=1 TO 3
```

```
4350 !
4360 !
4370 ! COMPUTING THE KALMAN GAIN
4380 !
4390       FOR N=1 TO 3
4400          PH(N)=PPR(N,1)*H(M,1)+PPR(N,2)*H(M,2)+PPR(N,3)*H(M,3)
4410       NEXT N
4420       V=H(M,1)*PH(1)+H(M,2)*PH(2)+H(M,3)*PH(3)+R2
4430       IF M=3 THEN V=V+R2
4440       GAIN(1)=PH(1)/V @ GAIN(2)=PH(2)/V @ GAIN(3)=PH(3)/V
4450 !
4460 !
4470 ! UPDATING THE STATE ESTIMATE VECTOR AND THE LOG-LIKELIHOOD
4480 ! FUNCTIONS IN EACH OF THE EIGHT FILTER ELEMENTS
4490 !
4500       FOR F=1 TO 8
4510           Z=ZM(M,I)-FX(F,M)
4520           TEMP=H(M,1)*XPR(F,1)+H(M,2)*XPR(F,2)
4530           RES=Z-(TEMP+H(M,3)*XPR(F,3))
4540           XPR(F,1)=XPR(F,1)+GAIN(1)*RES
4550           XPR(F,2)=XPR(F,2)+GAIN(2)*RES
4560           XPR(F,3)=XPR(F,3)+GAIN(3)*RES
4570           XLKHD(F)=XLKHD(F)+RES¢2/2/V
4580       NEXT F
4590 !
4600 !
4610 ! UPDATING THE STATE ERROR COVARIANCE MATRIX
4620 !
4630       FOR N=1 TO 3
4640          FOR NN=1 TO 3
4650             PKH(N,NN)=-(GAIN(N)*H(M,NN))
4660             IF N=NN THEN PKH(N,NN)=1+PKH(N,NN)
4670          NEXT NN
4680       NEXT N
4690       FOR N=1 TO 3
4700          FOR NN=1 TO 3
4710             TEMP=PKH(N,1)*PPR(1,NN)+PKH(N,2)*PPR(2,NN)
4720             P(N,NN)=TEMP+PKH(N,3)*PPR(3,NN)
4730          NEXT NN
4740       NEXT N
4750       FOR N=1 TO 3
4760          FOR NN=1 TO 3
4770             PPR(N,NN)=P(N,NN)
4780          NEXT NN
4790       NEXT N
4800    NEXT M
4810 NEXT I
4820 !
4830 !
4840 ! COMPARING THE LOG-LIKELIHOOD FUNCTIONS AMONG THE EIGHT ELEMENTS
```

```
4850 !
4860 NR=1 @ XMIN=XLKHD(1)
4870 FOR F=2 TO 8
4880    IF XLKHD(F)>= XMIN THEN 4900
4890    XMIN=XLKHD(F) @ NR=F
4900 NEXT F
4910 !
4920 !
4930 !   OUTPUT: THE STATE ESTIMATE OF THE TRUE FILTER ELEMENT
4940 !
4950 PRINT XPR(NR,1),XPR(NR,2),XPR(NR,3)
4960 END
4970 ! ##########################################################################
4980 !
4990 !
5000 ! THE SUBROUTINE "DRNCOS" COMPUTES THE DIRECTIONAL VECTORS
5010 ! IN 3-DIMENSIONAL SPACE FROM THE INITIAL SATELLITE ANGLES
5020 ! GIVEN THE ELAPSED TIME, DT.
5030 !
5040 DRNCOS:
5050    CA1=COS (ALFA1+DT) @ CA2=COS (ALFA2+DT)
5060    SA1=SIN (ALFA1+DT) @ SA2=SIN (ALFA2+DT)
5070    CB1=COS (BETA1+DT) @ CB2=COS (BETA2+DT)
5080    SB1=SIN (BETA1+DT) @ SB2=SIN (BETA2+DT)
5090    CT1=COS (THET1+DT/2) @ CT2=COS (THET2-DT/2)
5100    ST1=SIN (THET1+DT/2) @ ST2=SIN (THET2-DT/2)
5110    CX(1)=CA1*CT1+SA1*ST1/2 @ CY(1)=-(CA1*ST1)+SA1*CT1/2
5120    CZ(1)=.866*SA1
5130    CX(2)=CA2*CT1+SA2*ST1/2 @ CY(2)=-(CA2*ST1)+SA2*CT1/2
5140    CZ(2)=.866*SA2
5150    CX(3)=-(CB1*CT2)+SB1*ST2/2 @ CY(3)=-(CB1*ST2)-SB1*CT2/2
5160    CZ(3)=.866*SB1
5170    CX(4)=-(CB2*CT2)+SB2*ST2/2 @ CY(4)=-(CB2*ST2)-SB2*CT2/2
5180    CZ(4)=.866*SB2
5190 RETURN
```